Project 2457 | January 2026

SJSU SAN JOSÉ STATE UNIVERSITY

MTI MINETA TRANSPORTATION INSTITUTE

Numerical Modeling of Climate Change Impacts on Transportation Embankments

Amr M. Morsy, PhD, PE Mamata Sapkota Emma Varela Odalys Portillo

CSUTC California State University Transportation Consortium

CALIFORNIA STATE UNIVERSITY LONG BEACH

MINETA TRANSPORTATION INSTITUTE

Founded in 1991, the Mineta Transportation Institute (MTI), an organized research and training unit in partnership with the Lucas College and Graduate School of Business at San José State University (SJSU), increases mobility for all by improving the safety, efficiency, accessibility, and convenience of our nation's transportation system. Through research, education, workforce development, and technology transfer, we help create a connected world. MTI leads the California State University Transportation Consortium (CSUTC) funded by the State of California through Senate Bill 1 and the Climate Change and Extreme Events Training and Research (CCEETR) Program funded by the Federal Railroad Administration. MTI focuses on three primary responsibilities:

Research

MTI conducts multi-disciplinary research focused on surface transportation that contributes to effective decision making. Research areas include: active transportation; planning and policy; security and counterterrorism; sustainable transportation and land use; transit and passenger rail; transportation engineering; transportation finance; transportation technology; and workforce and labor. MTI research publications undergo expert peer review to ensure the quality of the research.

Education and Workforce Development

To ensure the efficient movement of people and goods, we must prepare the next generation of skilled transportation professionals who can lead a thriving, forward-thinking transportation industry for a more connected world. To help achieve this, MTI sponsors a suite of workforce development and education opportunities. The Institute supports educational programs offered by the Lucas Graduate School of Business: a Master of Science in Transportation Management, plus graduate certificates that include High-Speed and Intercity Rail Management and Transportation Security Management. These flexible programs offer live online classes so that working transportation professionals can pursue an advanced degree regardless of their location.

Information and Technology Transfer

MTI utilizes a diverse array of dissemination methods and media to ensure research results reach those responsible for managing change. These methods include publication, seminars, workshops, websites, social media, webinars, and other technology transfer mechanisms. Additionally, MTI promotes the availability of completed research to professional organizations and works to integrate the research findings into the graduate education program. MTI's extensive collection of transportation-related publications is integrated into San José State University's world-class Martin Luther King, Jr. Library.

Report 25-33

Numerical Modeling of Climate Change Impacts on Transportation Embankments

Amr M. Morsy, PhD, PE

Mamata Sapkota

Emma Varela

Odalys Portillo

January 2026

A publication of the
Mineta Transportation Institute
Created by Congress in 1991

College of Business
San José State University
San José, CA 95192-0219

TECHNICAL REPORT DOCUMENTATION PAGE

1. Report No. 25-33	**2. Government Accession No.**	**3. Recipient's Catalog No.**	
4. Title and Subtitle Numerical Modeling of Climate Change Impacts on Transportation Embankments		**5. Report Date** January 2026 **6. Performing Organization Code**	
7. Authors Amr Morsy: 0000-0002-9335-7847 Mamata Sapkota: 0009-0002-3054-2081 Emma Varela: 0009-0001-9931-3503 Odalys Portillo: 0009-0007-1244-8370		**8. Performing Organization Report** CA-MTI-2457	
9. Performing Organization Name and Address Mineta Transportation Institute College of Business San José State University San José, CA 95192-0219		**10. Work Unit No.** **11. Contract or Grant No.** SB1-SJAUX_2023-26	
12. Sponsoring Agency Name and Address State of California SB1 2017/2018 Trustees of the California State University Sponsored Programs Administration 401 Golden Shore, 5th Floor Long Beach, CA 90802		**13. Type of Report and Period Covered** **14. Sponsoring Agency Code**	
15. Supplemental Notes 10.31979/mti.2026.2457			
16. Abstract Embankments are essential components of transportation infrastructure, providing crucial support for long stretches of highways, railways, and other routes in California and around the world. Clay embankments are susceptible to weather-related deterioration processes that can gradually compromise their stability and, in some cases, lead to unexpected failures. Climate change, along with the associated shifts in weather patterns, is projected to adversely impact the weather-related deterioration processes, leading to exacerbated failures and/or shorter service life. Additionally, climate change is projected to increase the frequency of extreme precipitation events, leading to an increase in embankment failure potential. This study evaluated (1) the effect of future climate scenarios on the long-term performance of clay embankments, and (2) the effect of extreme precipitation events brought about by future climate scenarios on the hydromechanical response of clay embankments to these extreme events. This study examined areas in central Los Angeles, California. Multi-phase hydromechanical geotechnical models were developed for exemplary high plasticity and low plasticity clay embankments with varied side slope angles. Overall, it was concluded that climate change is generally projected to adversely affect the performance of clay embankments both in the long-term and during extreme events, which can negatively impact critical national transportation infrastructure and disrupt the movement of people and goods.			
17. Key Words Embankments, earthwork, climate change, weathering, deterioration by environmental action.	**18. Distribution Statement** No restrictions. This document is available to the public through The National Technical Information Service, Springfield, VA 22161.		
19. Security Classif. (of this report) Unclassified	**20. Security Classif. (of this page)** Unclassified	**21. No. of Pages** 80	**22. Price**

Form DOT F 1700.7 (8-72)

DOI: 10.31979/mti.2026.2457

Mineta Transportation Institute
College of Business
San José State University
San José, CA 95192-0219

Tel: (408) 924-7560
Fax: (408) 924-7565
Email: mineta-institute@sjsu.edu

transweb.sjsu.edu/research/2457

ACKNOWLEDGMENTS

This study was supported by the California State University Transportation Consortium (CSUTC) through California Senate Bill 1 (SB 1): The Road Repair and Accountability Act of 2017. The opinions presented in this report are those of the authors and are not necessarily those of the CSUTC. Amr Morsy recognizes the support of David (TM) Liao of the California State Department of Transportation (Caltrans) and Dr. Hilary Nixon of the Mineta Transportation Institute (MTI). The authors thank Lisa Rose/Editing Press for editorial services, as well as MTI staff Project Assistant Rajeshwari Rajesh and Graphic Design Assistant Katerina Earnest. Report cover photo belongs to ©Puckillustrations/AdobeStock.

Contents

LIST OF FIGURES

LIST OF TABLES

Executive Summary

Transportation embankments are responsible for supporting a large number of long-linear transportation infrastructure features including highways and railways, in California and globally. Clay embankments are susceptible to weather-related deterioration processes that can gradually compromise their stability and, in some cases, lead to unexpected failures, particularly in aging infrastructure. California's recent rainy season of 2017, following a five-year drought, has caused severe flooding, landslides, and coastal erosion, totalling over $1 billion in highway damages for the California Department of Transportation (Caltrans). Given that California plays a pivotal role as a major provider of goods and services to the broader United States, any disruption in its transportation system could result in calamitous repercussions for the entire nation, as per the California's Fourth Climate Change Assessment.

In a survey carried out by Beckstrand and Bunn (2024) through an NCHRP synthesis on surficial (i.e., shallow) embankment failures, California is responsible for approximately 15,092 road miles, of which around 40% are estimated to be susceptible to surficial failures. Approximately 80% of embankment failures in California are considered surficial (less than 3 m deep). Surficial embankment failures commonly occur following severe weather events or a sequence of events, a pattern that has also been observed in California. These types of failures typically occur in California embankments that are 20 to 40 years old, assuming they were designed and constructed appropriately.

Climate change, along with the associated shifts in weather patterns, is projected to adversely impact these weather-related deterioration processes, leading to exacerbated failures and/or shorter service life. Additionally, climate change is projected to increase the frequency of extreme precipitation events, leading to an increase in embankment failure potential. This study evaluated (1) the effect of perturbed future climate scenarios on the long-term performance of clay embankments and (2) the effect of extreme precipitation events brought about by perturbed future climate scenarios on the response of clay embankments to these extreme events. The study area selected in this study was central Los Angeles, California. This evaluation was conducted using advanced numerical models for exemplar high plasticity and low plasticity clay embankments with varied side slope angles. Overall, it was concluded that climate change is generally projected to adversely affect the performance of clay embankments both in the long-term and during extreme events.

The developed numerical models can simulate the long-term performance of embankments subject to climate-controlled flux boundaries. The models were used to perform numerical simulations with various climate perturbed parameter ensembles of ten future climate scenarios. A total of twenty-six numerical simulations were conducted to evaluate the long-term performance of embankments. A parametric evaluation was conducted to evaluate the effect of perturbed future climate scenarios on the long-term performance of clay embankments. This parametric evaluation

provided insights into the effect of climate change on the long-term performance of clay embankments. Notably, the results of this evaluation indicated that the rate of increase in irrecoverable vertical displacements reduced with time as soil swelling reached its potential, whereas the increase in irrecoverable outward displacement persisted with time. Swelling-induced shallow slides are likely triggered at this condition. In Los Angeles climate, this is likely to occur after 70–80 years in clay embankments with side slopes between 2:1 and 3:1 and after 20–40 years in clay embankments with side slopes between 1.5:1 and 2:1. Accordingly, it is recommended that existing embankments constructed from high plasticity clays that are older than these limits and whose failure consequences are high may require risk mitigation strategies, such as monitoring of side slope displacement and near-surface soil moisture.

The developed numerical models were also used to simulate the short-term performance of embankments subject to extreme precipitation events. Extreme precipitation events brought about by four perturbed climate scenarios with varied rainfall precipitation intensities and durations were simulated. A total of fifty-four numerical simulations were conducted to evaluate the short-term performance of embankments subject to extreme precipitation events. A parametric evaluation was conducted to evaluate the effect of extreme precipitation events brought about by perturbed future climate scenarios on the hydromechanical response of clay embankments to these extreme events. This parametric evaluation provided insights into the effect of climate change on the response of clay embankments to extreme events. Notably, the results of this evaluation indicated that high plasticity clay embankments are highly susceptible to extreme precipitation events with a 100-year return period (i.e., events with 1% annual exceedance probability), especially those with durations longer than 2 days. Extreme precipitation events are much less likely to have detrimental impacts on low plasticity clay embankments than on high plasticity clay embankments.

It is evident that numerical models that consider the influence of weather-related factors on the degradation and potential failure of earthworks, such as the one presented in this study, can provide insights into the behavior of transportation infrastructure that are prone to long-term weather-driven deterioration or are vulnerable to extreme events. Such insights can be of significant value for infrastructure asset management. Prediction of potential failures allows infrastructure stakeholders to plan timely intervention (e.g., maintenance, repair, rehabilitation) proactively, optimize their budget allocation, and reduce overall maintenance costs. These in turn can significantly increase the longevity of the infrastructure assets, leading to cost savings over the long term. Accordingly, a simplified framework was proposed to show how the work completed herein contributes to geotechnical asset management.

1. Introduction

Earthworks play a vital role in the transportation network, providing essential support for long-linear stretches of highways and railways. However, these earthworks are susceptible to weather-driven deterioration processes that can gradually compromise their stability and, in some cases, lead to unexpected failures, particularly in aging infrastructure (Postill et al., 2021; Morsy et al., 2023a; Helm et al., 2024). Slope failures in California during rainy years are common and account for annual losses of approximately $200 million for years in which rainfall exceeds 140% of normal amounts (Slosson & Larson 1995). California's recent rainy season of 2017, following a five-year drought, has caused severe flooding, landslides, and coastal erosion, totaling over $1 billion in highway damages for Caltrans (Caltrans, 2018). Given that California plays a pivotal role as a major provider of goods and services to the broader United States, any disruption in its transportation system holds the potential to unleash calamitous repercussions for the entire nation (Bedsworth et al., 2018).

1.1 Overview of the Problem

In a survey carried out by Beckstrand and Bunn (2024) through an NCHRP synthesis on surficial embankment failures, California is responsible for approximately 15,092 road miles, of which around 40% are estimated to be susceptible to surficial failures. Approximately 80% of embankment failures in California are considered surficial (less than 3 m deep). In California surficial embankment failures commonly occur following severe weather events or a sequence of events. These types of failures typically occur in California embankments that are 20 to 40 years old, assuming they were designed and constructed appropriately.

Time-dependent deterioration of soil properties affects the long-term performance of infrastructure assets supported by soil slopes. It is evident that weather-driven deterioration mechanisms play a key role in the overall degradation of earth infrastructure assets. This may result in progressive weakening and collapse, particularly in clay embankment slopes (e.g., Templeton et al., 1984; Vaughan et al., 2004; Nyambayo et al., 2004; Rouainia et al., 2009; Nyambayo & Potts, 2010; Kovacevic et al., 2013; Morsy et al., 2023a; Morsy & Helm, 2024a). Shifts in weather patterns brought about by climate change are projected to further exert adverse impacts on the hydromechanical behavior of geotechnical infrastructure, including earthworks, and on the rate of their weather-driven deterioration (Helm et al., 2024).

Additionally, embankment slopes can collapse when subject to extreme rainfall events or a repeated sequence of events. The frequency of such events is projected to increase in the future due to climate change. During such heavy rainfall events, embankment deterioration can exacerbate, leading to failure (e.g., Linrong et al., 2023; Fan et al., 2025). The hydromechanical response of earthen structures to extreme precipitation events can be analyzed using precipitation intensity-

duration-frequency (IDF) curves (Cheng & AghaKouchak, 2014; Robinson et al., 2016; Vahedifard et al., 2017).

The California Department of Transportation (Caltrans) has developed plans to assess how climate change impacts the state's transportation infrastructure to improve its resilience and protect it from potential damage. These efforts align with state efforts to "translate the state of climate science into useful information for decision-makers and practitioners" across the state (Caltrans, 2018, p. 3), as per the California's Fourth Climate Change Assessment (Bedsworth et al., 2018).

Weather-driven deterioration models for earthworks are important for understanding how climate and environmental conditions affect the stability and lifespan of the infrastructure assets built on these earthworks. These deterioration models usually depend on real-time or historical field data to support decisions in asset management. However, such data are often scarce or inadequate to extrapolate to a wide range of assets. To address this, robust modeling tools are needed to reliably predict how these structures will perform in the future and estimate their remaining service life, especially under different climate change scenarios.

1.2 Research Objectives

This study aimed to assess the impact of climate change on the hydromechanical behavior of transportation embankments in California under long-term, gradual weather-driven deterioration and under short-term extreme events brought about by future perturbed climate scenarios. Specifically, this study used a numerical modeling approach developed and validated by Morsy et al. (2023a, 2023b) and Morsy and Helm (2024a, 2024b) to simulate the hydromechanical behavior of exemplary transportation embankments subject to a controlled climate flux. Two groups of parametric evaluations were conducted to evaluate the long-term and short-term hydromechanical behavior of clay embankments under future climate scenarios:

1) A parametric evaluation was performed to evaluate the effect of perturbed future climate scenarios on the long-term performance of clay embankments, including the effect of average annual precipitation change, extreme precipitation quantile change, and temperature change. The evaluation involved exemplary embankments constructed from high plasticity and low plasticity clays, with side slopes of 3.0:1, 2.0:1, and 1.5:1 (run to rise). The simulations were performed under climate suites from 2020 through 2100.

2) A parametric evaluation was performed to evaluate the effect of extreme precipitation events brought about by perturbed future climate scenarios on the hydromechanical response of clay embankments to these extreme events. The parametric evaluation involved studying the effect of the extreme event precipitation intensity and duration, the effect of slope inclination, and the effect of soil type. The evaluation involved exemplary embankments constructed from high plasticity and low plasticity clays, with side slopes of

3.0:1, 2.0:1, and 1.5:1 (run to rise). The simulations were performed under 1-day, 3-day, and 7-day extreme precipitation events with a 100-year return period.

1.3 Report Organization

This report consists of the following sections:

3) Section 1. Introduction. This section presents an overview of the problem and research questions, research aim and objectives, and report organization.

4) Section 2. Numerical Model. This section presents the development of the numerical model.

5) Section 3. Perturbed Climate of Los Angeles. This section documents the perturbed climate suites generated to simulate future climate conditions in California.

6) Section 4. Long-Term Performance of Earth Embankments under Perturbed Climate Patterns. This section presents and discusses the results of the parametric evaluation of the embankments' long-term performance under various future climate scenarios.

7) Section 5. Short-Term Performance of Earth Embankments under Perturbed Extreme Events. This section presents and discusses the results of the parametric evaluation of the embankments' short-term performance under extreme events brought about by various future climate scenarios.

8) Section 6. The Prospective Role of Performance Numerical Modeling in Geotechnical Asset Management. This section explains how the work completed in this study contributes to geotechnical asset management.

9) Section 7. Summary and Conclusions. This section summarizes the studies documented in this report and provides practical recommendations based on their findings.

2. Numerical Model

This study used a numerical modeling approach previously developed by Morsy et al. (2023a) specifically for simulating the weather-driven deterioration of embankments. This modeling approach has undergone validation, demonstrating its effectiveness in capturing the long-term hydromechanical behavior of embankments (Morsy et al., 2023a, 2023b). The validation process involved a comprehensive study using a full-scale research embankment equipped with 9 years of monitoring data, including parameters such as soil moisture, matric suction, and settlement. Additionally, the modeling approach was validated based on its ability to predict the service life (i.e., time to failure) for 34 well-documented embankment failure case histories (Morsy & Helm, 2024a, 2024b).

The embankment numerical model was developed using FLAC (Fast Lagrangian Analysis of Continua) software v8.1. This software was used to run hydromechanical simulations to study the behavior of the modeled embankment under various climate scenarios. A detailed description of the model development is provided by Morsy et al. (2023a). A detailed description of the boundary conditions and initial conditions adopted for the embankment models is provided by Morsy and Varela (2025).

2.1 Mechanical Behavior

The mechanical behavior of the fill materials was modeled using a multi-stage Mohr-Coulomb model with strain softening to simulate the change in mechanical behavior of clays with time. Mohr-Coulomb parameters (cohesion intercept, c; angle of internal resistance, ϕ; and angle of dilation, ψ) varied with accumulated ratcheting plastic strain and with seasonal wet-dry cycles in the near surface. A detailed description of the model is provided in Morsy and Helm (2024a).

Young's modulus of the soil, E, was defined as a function in mean effective stress, σ'_m, as suggested by Kulhawy et al. (1969):

$$E = E_o p_o \left(\frac{\sigma'_m}{p_o}\right)^{m_E}, \frac{\sigma'_m}{p_o} \geq 0.1 \qquad (1)$$

where E_o is Young's modulus at 1 atm, p_o is the atmospheric pressure (1 atm), and m_E is the Young's modulus stress exponent. Poisson's ratio, υ, of the soil was defined as a function in mean effective stress, $\sigma_m{}'$, as suggested by Kulhawy et al. (1969):

$$\upsilon = \upsilon_o - \ln\left(\frac{\sigma'_m}{p_o}\right)^{m_\upsilon}, \frac{\sigma'_m}{p_o} \geq 0.1 \qquad (2)$$

where υ_o is Poisson's ratio at 1 atm, p_o is the atmospheric pressure, and m_υ is the Poisson's ratio stress exponent. Mean effective normal stresses, σ'_m, were modeled based on Bishop's generalized effective stress (Bishop 1959):

$$\sigma'_m = \sigma_m - u_a + \chi(u_a - u_w) \qquad (3)$$

where σ_m is the mean total normal stress, u_a is the pore-air pressure, u_w is the pore-water pressure, and χ is Bishop's effective stress parameter, and can be approximated to the degree of water saturation, S_w.

2.2 Hydraulic Behavior

Fluid transport in the finite-difference code used in this study is described by Darcy's law (Itasca, 2019). The soil-water retention curve was developed based on field measurements and were represented using the van Genuchten (1980) fitting model for both the embankment fill and the foundation soil, as follows:

$$\psi_m = \psi_{m,o}\left(S_e{}^{-1/a_{vg}} - 1\right)^{1-a_{vg}} \qquad (4)$$

where ψ_m is the matric suction, $\psi_{m,o}$ is a fitting parameter related to the air-entry matric suction, and a_{vg} is a fitting parameter. S_e is the effective saturation, expressed as $S_e = (S_w - S_{w,r})/(1 - S_{w,r})$, where $S_{w,r}$ is the residual degree of water saturation. The model treats pore fluids as two immiscible fluids whose volumes make up the total void volume. Accordingly, the degree of air saturation, S_g, can be expressed as $S_g = 1 - S_w$.

The hydraulic conductivity function was correlated to the soil-water retention curve using the van Genuchten-Mualem model (Mualem, 1976; van Genuchten, 1980) as $k_w = \kappa_{r,w}\, k_{w,sat}$, where k_w is the hydraulic conductivity, $k_{w,sat}$ is k_w at $S_w = 1$, and $\kappa_{r,w}$ is the relative conductivity, which can be expressed as follows:

$$\kappa_{r,w} = S_e{}^{0.5}\left[1 - \left(1 - S_e{}^{1/a_{vg}}\right)^{a_{vg}}\right]^2 \qquad (5)$$

The air conductivity function was correlated to the hydraulic conductivity function (Parker et al., 1987) as $k_g = \kappa_{r,g}\, k_{g,sat}$, where k_g is the air conductivity, and $k_{g,sat}$ is k_g at $S_w = 1$, which was correlated to the saturated hydraulic conductivity using fluid unit weights and dynamic viscosities, as $k_{g,sat} = \left[(\gamma_g\, \mu_w)/(\gamma_w\, \mu_g)\right] k_{w,sat}$, and $\kappa_{r,g}$ is the relative air conductivity, which can be expressed as follows:

$$\kappa_{r,g} = (1 - S_e)^{0.5}\left(1 - S_e{}^{1/a_{vg}}\right)^{2a_{vg}} \qquad (6)$$

The saturated hydraulic conductivity, $k_{w,sat}$, was correlated to the void ratio, e, according to the empirical formula proposed by Samarasinghe *et al.* (1982) as $k_{w,sat} = C\, e^l/(1 + e)$, where C and l are empirical parameters that depend on the clay mineralogy.

2.3 Embankment Parameters

As discussed in Morsy and Varela (2024), according to a survey conducted by Beckstrand and Bunn (2024) as part of an NCHRP synthesis on surficial embankment failures, California does not maintain inventories of embankment attributes (height, length, side-slope angles, material, year of construction). Accordingly, this study derived ranges of embankment attributes for a typical high plasticity clay (CH) fill and a typical low plasticity clay (CL) fill, which are sensitive fills to weather-driven deterioration. Table 1 summarizes the parameters of the mechanical and hydraulic models adopted for the two fills modeled in this study. Figure 1 shows the variation of the angle of internal resistance and cohesion intercept with plastic strain. Figure 2 shows the fluid retentivity and conductivity models.

Table 1. Parameters of Mechanical and Hydraulic Models

Parameter		Parameter Ranges			Selected Values	
		CH (LL = 80; 44 < PI < 64)	CL (LL = 40; 15 < PI < 28)	Reference	CH	CL
Standard Proctor maximum dry unit weight	$\gamma_{d,max}$ (kN/m^3)	14.8 ± 0.3	17.0 ± 0.2	Samtani and Nowatzki (2021)	15.1	17
Standard Proctor optimum moisture content	w_{opt} (%)	25.5 ± 1.2	17.3 ± 0.3	Samtani and Nowatzki (2021)	24.7	17
Void ratio	e (-)	0.80 ± 0.04	0.59 ± 0.01	Samtani and Nowatzki (2021)	0.786	0.59
Peak friction angle	$\phi_p^{'}$ (˚)	19 ± 5	28 ± 2	Samtani and Nowatzki (2021)	19	28
Peak cohesion intercept	$c_p^{'}$ (kPa)	11 ± 6	13 ± 2	Samtani and Nowatzki (2021)	11	13
Critical state friction angle	$\phi_{cs}^{'}$ (˚)	19 to 26	22 to 29	Stark *et al.* (2005)	19	28
Critical state cohesion intercept	$c_{cs}^{'}$ (kPa)	0	0	-	0	0
Residual friction angle	$\phi_r^{'}$ (˚)	9 to 12	16.5 to 20.5	Stark *et al.* (2005)	10	18.5
Residual cohesion intercept	$c_r^{'}$ (kPa)	0	0	-	0	0
Young's modulus at reference stress 1 atm	E_o (kPa)	230 to 400	240 to 360	Morsy et al. (2023a); Morsy and Helm (2024a)	300	300
Young's modulus stress exponent	m_E (-)	0.25 to 0.35	0.25 to 0.54	Morsy et al. (2023a); Morsy and Helm (2024a)	0.3	0.3
Poisson's ratio at reference stress 1 atm	υ_o (-)	0.3	0.2	Morsy et al. (2023a); Morsy and Helm (2024a)	0.3	0.3
Poisson's ratio stress exponent	m_υ (-)	0.01 to 0.02	0.05	Morsy et al. (2023a); Morsy and Helm (2024a)	0.01	0.01
Saturated Hydraulic Conductivity	$k_{w,sat}$ (m/s)	(5±5)×10^{-10}	(8±3)×10^{-10}	Samtani and Nowatzki (2021)	$k_{w,sat} = 1 \times 10^{-8} = \left(\frac{e^5}{1+e}\right)$	
Soil-Water Retention Model Fitting Parameter	a_{vg} (-)	-	-	Morsy et al. (2023a); Morsy and Helm (2024a)	0.23	0.23
Soil-Water Retention Model Fitting Parameter	$\psi_{m,o}$ (kPa)	-	-	Morsy et al. (2023a); Morsy and Helm (2024a)	300	200
Residual Degree of Water Saturation	$S_{w,r}$ (-)	0	0	Morsy et al. (2023a); Morsy and Helm (2024a)	0	0

Figure 1. Shear Strength Model: (a) Variation of the Angle of Internal Resistance with Deviatoric Plastic Strain; and (b) Variation of the Cohesion Intercept with Deviatoric Plastic Strain. Cohesion Intercept Peak is Allowed to Reduce with Seasonal Wet-Dry Cycles

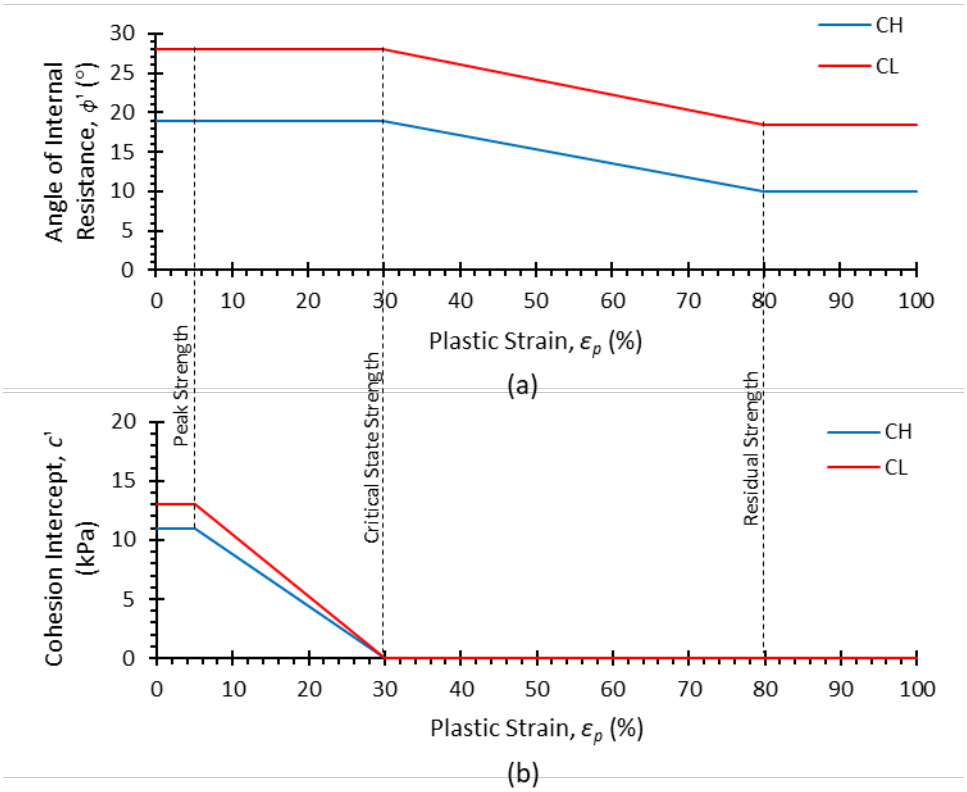

Figure 2. Fluid Models: (a) Fluid Retentivity Models and (b) Fluid Conductivity Models

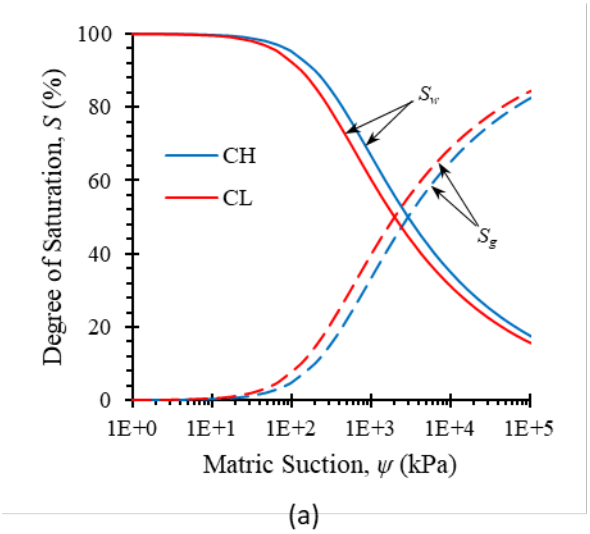

(a)

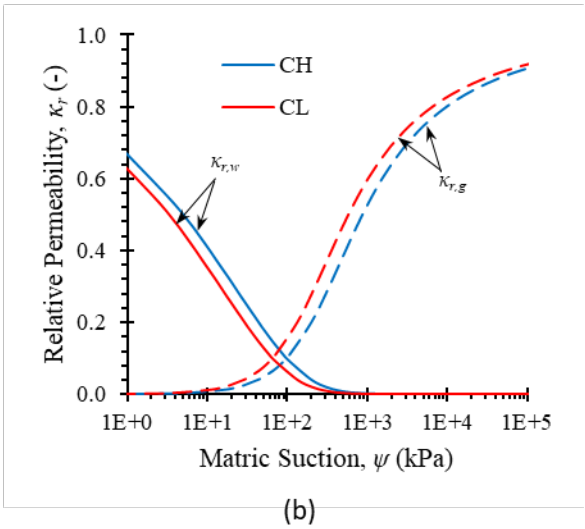

(b)

As discussed in Morsy and Varela (2024), the embankment model geometry was derived from the embankment design specifications and common practice in California. A target side slope would be the desired slope if no right-of-way or foundation constraints were to influence embankment design. A commonly used target side slope is 4H:1V, which the FHWA generally considers a recoverable slope (Beckstrand & Bunn, 2024). In California, 4H:1V is the recommended target side slope for embankments per California Landscape Architecture unit and the maximum recommended side slope is 1.5H:1V per California Geotechnical unit. The Caltrans Highway Design Manual (Caltrans, 2020) specifies that embankment end slopes at open end structures should not be steeper than 1.5H:1V for all highways. Based on this information, this study used embankment models with side slopes 3.0:1, 2.0:1, and 1.5:1 (run to rise).

Additionally, as per the Caltrans Highway Design Manual (Caltrans, 2020), embankments shorter than 3 m with side slopes 2H:1V or flatter may be designed based on past precedence and engineering judgment, provided there are no known problem soil conditions such as organic soils,

soft/loose soils, potentially unstable soils such as Bay Mud or peat, or liquefiable sands. In-depth stability analyses are required for embankments taller than 3 m, embankments with side slope 2H:1V or steeper, embankments on soft soils, embankments in unstable areas/soils, or embankments constructed from lightweight fills. Based on this information, this study used embankment models of height 6 m, which is twice the limit of embankments that do not require in-depth analysis.

3. Perturbed Climate of Los Angeles

The study area selected for this study is Los Angeles, CA. The climate of Los Angeles is classified as *Warm-Summer Mediterranean (Csb)* per the Köppen climate classification, *South Coast* per Caltrans pavement climate regions and CA DWR hydrologic regions, and *Upland Central Coast and Los Angeles Basin (Higher elevation coastal areas)* per the California Irrigation Management Information System (CIMIS) reference evapotranspiration zones. Suites of Climate Perturbed Parameter Ensembles (PPEs) were developed for the study area using the weather generator by Najibi and Steinschneider (2023), which was developed for the California Department of Water Resources (CA DWR).

3.1 Generation of Future Weather Predictions

The weather generator developed by Najibi and Steinschneider (2023) assumed that the temperature change can be treated by adding step changes to baseline daily maximum and minimum temperature data, which have already been processed to account for recent warming, uniformly across the entire spatial domain. They inferred this range of temperature increase from an ensemble of climate model projections selected by the CA DWR Climate Change Technical Advisory Group (CA DWR, 2015), which were taken from a subset of ten high performing GCMs for California from the CMIP5 archive. These projections suggested that +5˚C was the likely maximum warming expected by the end of the 21st century under the Representative Concentration Pathway (RCP) 8.5 emission scenario (Najibi & Steinschneider, 2023).

This study selected a total of ten climate scenarios, summarized in Table 2, to investigate the effects of average annual precipitation change, extreme precipitation quantile change, and temperature change on the long-term performance of clay embankments. Four of the climate scenarios were used to investigate the effect of extreme precipitation quantile change on the short-term performance of clay embankments during 100-year extreme precipitation events.

Table 2. Select Climate Scenarios from Najibi and Steinschneider (2023) Used in Developing Statewide, Weather-Regime Based Stochastic Weather Generator for California

Scenario No.	Incremental Temperature Change (℃)	% Change Extreme Precipitation Quantile	% Change Precipitation Mean
1	0	0	0
11	+1	+7	0
12	+2	+7	0
13	+3	+7	0
14	+4	+7	0
15	+5	+7	0
25	+3	0	–12.5
26	+3	0	0
27	+3	0	+12.5
29	+3	+14	0

The weather generator had two datasets: synthetic weather data from the past 100 years and synthetic weather data for the next 1,000 years. Data were downloaded from the past 100-year dataset to compare the weather generator predictions to actual climate data from local weather stations at the locations of the selected sites (Morsy & Varela, 2025). Data were downloaded from the future 1,000-year dataset for the climate scenarios studied herein, from which data spanning 2020 through 2100 were curated for each climate scenario. The grid element at coordinates 34.03125, –118.15625 was selected because of its relative proximity to the city center of Los Angeles compared to other adjacent grids.

Climate data was used to estimate reference evapotranspiration, ET_0, using the Penman-Monteith method as per FAO56 (Allen et al., 1998) for reference grass, which can be written as follows:

$$ET_0 = \frac{0.408\,\Delta\,(R_n - G) + \gamma\,\frac{900}{T+273}\,u_2\,(e_s - e_a)}{\Delta + \gamma\,(1 + 0.34\,u_2)} \qquad (7)$$

where R_n is the net radiation at the crop surface in MJ/m²/day; G is the soil heat flux density in MJ/m²/day; T is the mean daily air temperature at 2 m height in ˚C; u_2 is the wind speed at 2 m height in m/s; e_s is the saturation vapor pressure in kPa; e_a is the actual vapor pressure in kPa; Δ is the slope of vapor pressure curve in kPa/˚C; and γ is the psychometric constant in kPa/˚C. Refer to Allen et al. (1998) for more details.

The Gridded Weather Generator datasets only offered predictions for the minimum and maximum temperatures and precipitation. To calculate ET_0, additional data and assumptions were required. The solar radiation, R_s, was estimated based on the calculated extraterrestrial radiation, R_a, as follows (Allen et al., 1998):

$$R_s = k_{Rs} R_a \sqrt{(T_{max} - T_{min})} \qquad (8)$$

where T_{max} and T_{min} are the maximum and minimum temperatures in ˚C, and k_{Rs} is an adjustment coefficient that was taken herein as 0.16. The extraterrestrial radiation, R_a, is calculated based on the geographic location and the day of the calendar year, J, as follows:

$$R_a = \frac{1}{\pi} G_{sc}\, d_r\, (\omega_s \sin\varphi \sin\delta + \cos\varphi \cos\delta \sin\omega_s) \qquad (9)$$

where G_{sc} is the solar constant = 0.082 MJ/m²/min; d_r is the inverse relative distance Earth-Sun and can be calculated as $d_r = 1 + 0.033 \cos\left(\frac{2\pi J}{365}\right)$; ω_s is the sunset hour angle and can be calculated as $\omega_s = \cos^{-1}(-\tan\varphi \tan\delta)$; φ is the latitude; and δ is the solar inclination and can be calculated as $\delta = 0.409 \sin\left(\frac{2\pi J}{365} - 1.39\right)$. Refer to Allen et al. (1998) for more details.

In absence of future relative humidity predictions, the actual vapor pressure, e_a, was estimated based on the dewpoint temperature, T_{dew} as follows (Allen et al., 1998):

$$e_a = 0.6108 \exp\left(\frac{17.27\, T_{dew}}{237.3 + T_{dew}}\right) \qquad (10)$$

T_{dew} can be estimated in ˚C based on the maximum and minimum temperatures as follows (Linacre, 1992):

$$T_{dew} = (0.52)T_{min} + (0.6)T_{max} - (0.009)T_{max}^2 - 2 \qquad (11)$$

Future wind speed data were obtained from the GFDL SPEAR Large Ensembles (Delworth et al., 2020). It is akin to the California weather generator in that it has a folder for past data which span the years 1921 to 2014 and a folder for future data which span the years 2015 to 2100. The past dataset was used with the aid of ArcGIS Pro. Within the software, a table of data was generated, listing dates in year-month format alongside corresponding wind speed values. This was then integrated into the curated datasets. Data were downloaded for the same coordinates (i.e., locations) of the selected site in Los Angeles. Wind speed was assumed to be the same in all local climate scenarios studied herein.

To validate the use of the weather generator predictions without climate bias correction, predicted weather parameters from the weather generator were compared to observed historical records from the Los Angeles Downtown weather station located at 34.0678, –118.2417. It was concluded that the weather generator could reproduce past weather data well and was hence projected to produce reasonable future estimates without bias correction (see details in Morsy & Varela, 2025).

It is notable that the weather data obtained from the weather generator did not show significant shifts in weather patterns or gradual changes in temperature and mean precipitation over time. Instead, the weather generator assumed that the changes in temperature and mean precipitation are constant and incremental that has taken effect.

3.2 Generation of Intensity-Duration-Frequency Curves

The precipitation intensity-duration-frequency (IDF) curves were derived from the daily precipitation data for the future 1,000 years for the various perturbed climate scenarios. The extreme precipitation values were calculated using a simple ranking method. For each specified rainfall event duration (1, 2, 3, 5, and 7 days), the precipitation data were aggregated over different durations using a moving sum (with a forward-looking moving window equivalent to the respective event duration). The aggregated precipitation data were then sorted in descending order, and the empirical return level was obtained for each specified return period (2, 5, 10, 25, 50, and 100 years) from the value at the rank corresponding to the ratio of the total number of data points to the respective return period. The extreme event intensities were obtained by dividing the obtained return levels by each event duration. This approach, while simple, was deemed suitable for this study given the large dataset size (1,000 years of daily precipitation).

In this study, climate scenarios 26, 13, and 29 were selected to evaluate the sensitivity of extreme precipitation to climate change while controlling other variables. The change in extreme precipitation quantile was projected at 0%, +7%, and +14% for climate scenarios 26, 13, and 29, respectively. All three scenarios involved the same incremental temperature change of +3°C and no change in mean annual precipitation. Figure 3 presents the IDF curves for the 100-year return period extreme events derived for the three climate scenarios in Los Angeles (LOS26, LOS13, and LOS29).

Figure 3. Typical Intensity-Duration-Frequency (IDF) Curves Derived for Climate Scenarios (a) LOS26, (b) LOS13, and (c) LOS29

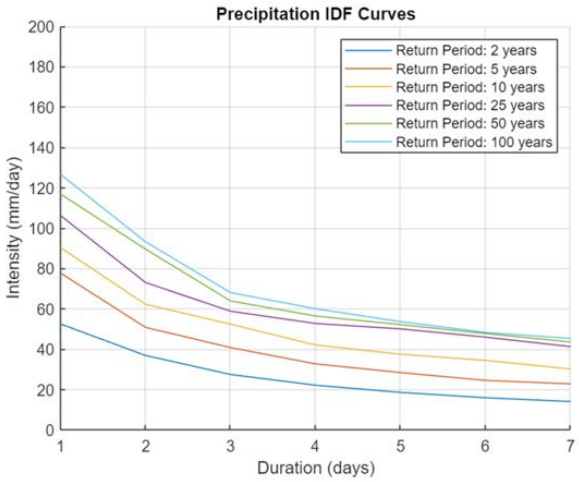

(a)

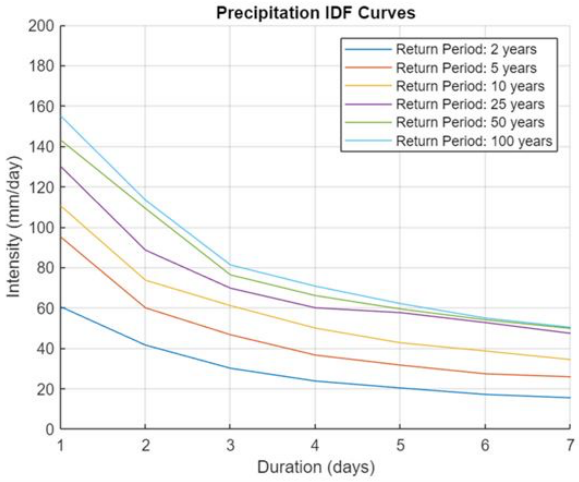

(b)

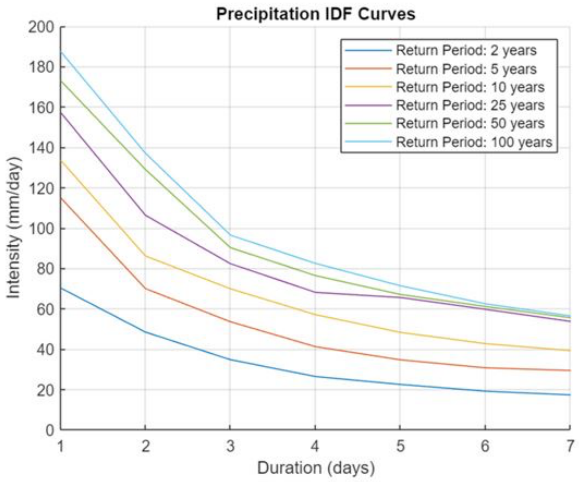

(c)

3.3 Climate Incorporation in Numerical Model

A transient climate boundary was defined at the surface of the model to simulate soil-atmosphere interaction. The climate boundary calculates the daily surface available net flux as the difference between precipitation and evapotranspiration in each simulation day. The daily available net flux values were divided uniformly over 24 hours and input in the climate boundary subroutine at every surface mesh node as it executed every one simulation hour to determine a boundary flux based on each node's pore pressure and saturation condition, as shown in Figure 4. A detailed description of this procedure is available in Morsy et al. (2023a).

Figure 4. Ground Surface Moisture Flux (Adapted from Fredlund Et Al. 2012)

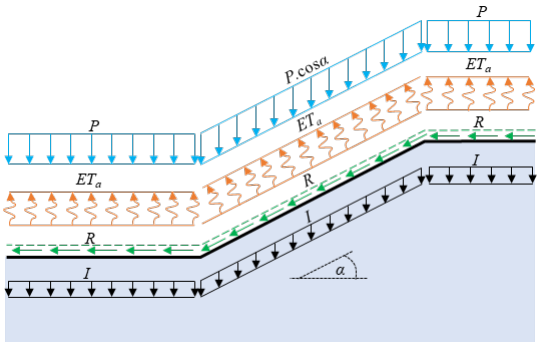

4. Long-Term Performance of Earth Embankments under Perturbed Climate Patterns

A parametric evaluation was conducted to evaluate the effect of perturbed future climate scenarios on the long-term performance of clay embankments, including the effect of average annual precipitation change, extreme precipitation quantile change, and temperature change. The evaluation involved exemplary embankments constructed from high plasticity and low plasticity clays, with side slopes of 3.0:1, 2.0:1, and 1.5:1 (run to rise). The baseline case was selected to be a high plasticity clay (CH) embankment 6 m in height with side slopes 3.0:1 (see Morsy & Varela, 2025). The simulations were performed under climate suites from 2020 through 2100. Some simulations were terminated earlier if the slope sustained failure or excessive deformation.

Simulations were given IDs to denote their geographical location and climate scenario. For example, an embankment constructed in Los Angeles and subjected to climate scenario 1 is given an ID of LOS01.

4.1 Effect of Average Annual Precipitation

To evaluate the effect of average annual precipitation on the long-term performance of clay embankments, numerical simulations were conducted on the baseline embankment model under climate scenarios 25, 26, and 27. These climate scenarios involved a change in future average annual precipitation of −12.5%, 0%, and +12.5%, respectively. These three scenarios also involved an incremental increase in future temperature of +3˚C and a change in extreme precipitation quantile of 0%. Additionally, a simulation was conducted with the baseline climate scenario 1, which assumed no climate change will take place in the future. Table 3 summarizes the parameters of the simulations discussed in this section. The results of these simulations were presented in Morsy and Varela (2025).

Table 3. Summary of the Long-Term Simulations Conducted to Evaluate the Effect of Average Annual Precipitation

Climate Scenario	Change in Incremental Temperature (˚C)	% Change in Extreme Precipitation Quantile	% Change in Precipitation Mean	Side Slope	Soil Type
1 (baseline)	0	0	0	3.0:1	CH
25	+3	0	−12.5	3.0:1	CH
26			0		
27			+12.5		

Figure 5 presents the time histories of the predicted mid-slope matric suction at depth 1 m for simulations LOS01, LOS25, LOS26, and LOS27. When comparing the numerical predictions of LOS01 and LOS26, the increase in future temperature by +3°C without a change in future mean precipitation would result in an overall slightly drier slopes as indicated by the higher near-surface matric suction observed in LOS26 compared to LOS01. An approximate 9% increase was observed in the predicted near-surface matric suction under climate scenario 26 in comparison to that under climate scenario 1.

When comparing the numerical predictions of LOS25, LOS26, and LOS27, it was observed that the near-surface matric suction would likely decrease (wetter slopes) with increasing the change in future mean precipitation. The difference in predicted matric suction between LOS27 simulation (+12.5% change in mean precipitation) and LOS25 (–12.5% change in mean precipitation) is approximately –15%. The difference in predicted matric suction between LOS27 simulation (+12.5% change in mean precipitation) and LOS26 (0% change in mean precipitation) is approximately –6%.

Figure 5. Predicted Time Histories of Mid-Slope Matric Suction at Depth 1 M from the Slope Surface for Climate Scenarios 1, 25, 26, and 27 (Morsy and Varela 2025)

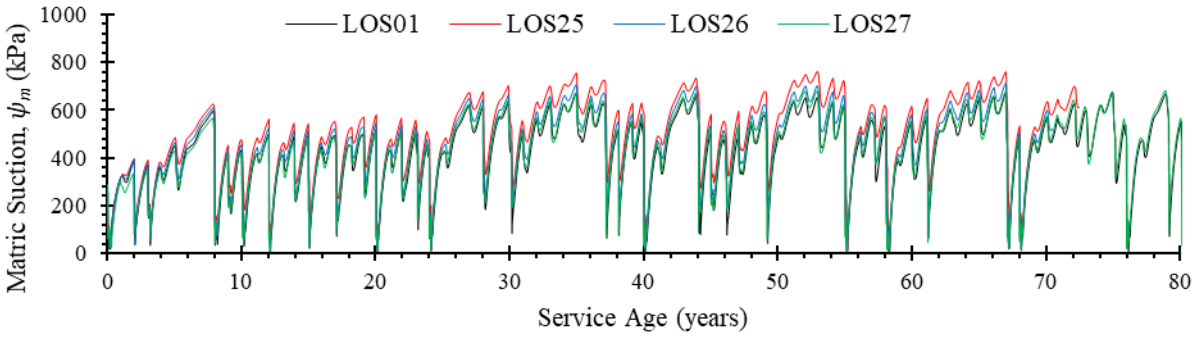

Figure 6 presents the time histories of the predicted mid-slope outward displacement at the slope surface for simulations LOS01, LOS25, LOS26, and LOS27. It is notable that the numerical model was able to capture the seasonal variation in outward displacements. During every wet season, an outward displacement took place, part of which recovered during the subsequent dry season. After every wet-dry cycle, an irrecoverable displacement (permanent deformation) accumulated over time. Note that the time histories in Figure 6 of all models under the various climate scenarios followed the same trend with different magnitudes, which is an artifact of the climate parameters predicted by the weather generator, as discussed earlier.

When comparing the numerical predictions of LOS01 and LOS26, it was observed that the increase in future temperature by +3°C without a change in future mean precipitation would result in slightly less outward displacement overall. This is attributed to the drier slopes (with higher matric suction and effective stress) under elevated future temperature and no change in mean precipitation, as discussed earlier. An approximate 15% decrease was observed in the predicted

mid-slope outward displacement under climate scenario 26 in comparison to that under climate scenario 1.

When comparing the numerical predictions of LOS25, LOS26, and LOS27, it was observed that the mid-slope outward displacement would likely increase with increasing the change in future mean precipitation, especially later in the service life as irrecoverable outward displacements accumulate. The difference in predicted mid-slope outward displacement between LOS27 simulation (+12.5% change in mean precipitation) and LOS25 (–12.5% change in mean precipitation) was approximately +31%. The difference in predicted mid-slope outward displacement between LOS27 simulation (+12.5% change in mean precipitation) and LOS26 (0% change in mean precipitation) was approximately +26%.

Figure 6. Predicted Time Histories of Mid-Slope Outward Displacement at the Slope Surface for Climate Scenarios 1, 25, 26, and 27 (Morsy and Varela 2025)

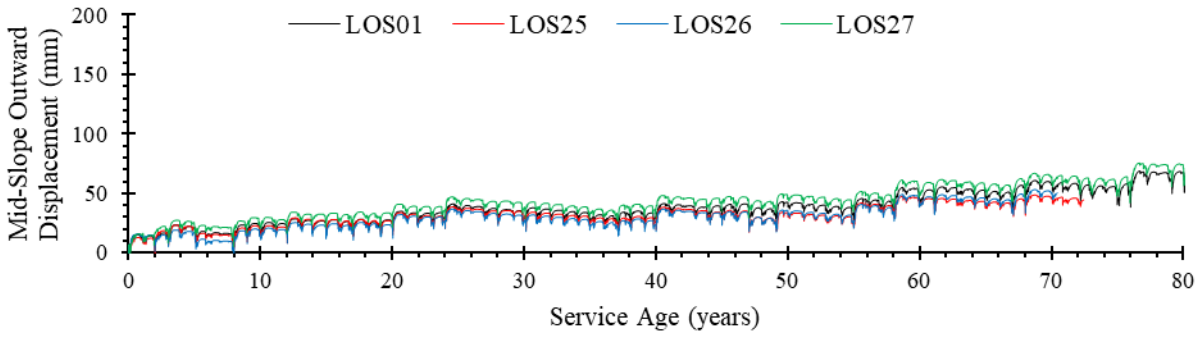

Figure 7 presents the time histories of the predicted mid-slope vertical displacement at the slope surface for simulations LOS01, LOS25, LOS26, and LOS27. Like outward displacements, the numerical model was able to capture the seasonal variation in vertical displacements. During every wet season, a vertical displacement (swelling) took place, part of which recovered during the subsequent dry season (shrinkage). After every wet-dry cycle, an irrecoverable swelling (permanent deformation) accumulated over time. Again, the time histories in Figure 7 of all models under the various climate scenarios followed the same trend with different magnitudes.

When comparing the numerical predictions of LOS01 and LOS26, it was observed that the increase in future temperature by +3˚C without a change in future mean precipitation would result in an insignificant difference in vertical displacement.

When comparing the numerical predictions of LOS25, LOS26, and LOS27, it was observed that the mid-slope vertical displacement would likely increase with increasing the change in future mean precipitation, especially later in the service life as irrecoverable vertical displacements accumulate. The difference in predicted vertical displacement between LOS27 simulation (+12.5% change in mean precipitation) and LOS25 (–12.5% change in mean precipitation) was approximately +13%. The difference in predicted vertical displacement between LOS27 simulation

(+12.5% change in mean precipitation) and LOS26 (0% change in mean precipitation) was approximately +7%.

Figure 7. Predicted Time Histories of Mid-Slope Vertical Displacement at the Slope Surface for Climate Scenarios 1, 25, 26, and 27 (Morsy and Varela 2025)

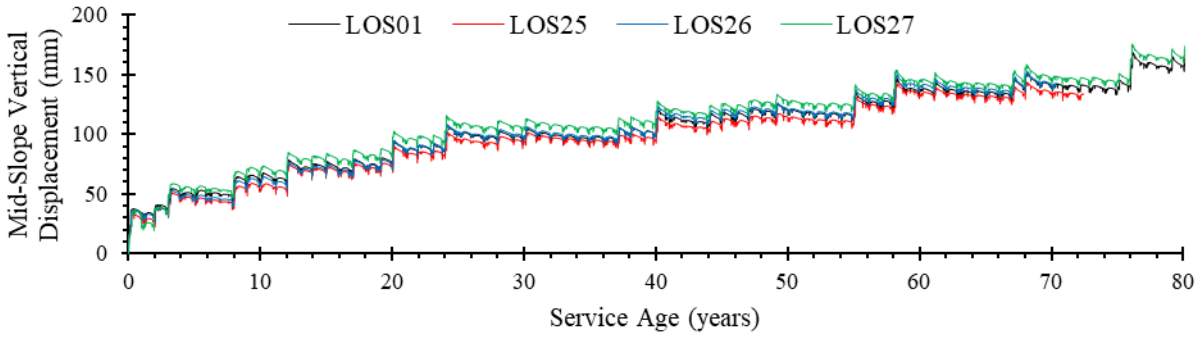

4.2 Effect of Extreme Precipitation Quantile

To evaluate the effect of extreme precipitation quantile on the long-term performance of clay embankments, numerical simulations were conducted on the baseline embankment model under climate scenarios 26, 13, and 29. These climate scenarios involved a change in future extreme precipitation quantile of 0%, +7%, and +14%, respectively. These three scenarios also involved an incremental increase in future temperature of +3˚C and a change in average annual precipitation of 0%. Table 4 summarizes the parameters of the simulations discussed in this section.

Table 4. Summary of the Long-Term Simulations Conducted to Evaluate the Effect of Extreme Precipitation Quantile

Climate Scenario	Change in Incremental Temperature (˚C)	% Change in Extreme Precipitation Quantile	% Change in Precipitation Mean	Side Slope	Soil Type
26	+3	0	0	3.0:1	CH
13		+7			
29		+14			

Figure 8 presents the time histories of the predicted mid-slope matric suction at depth 1 m for simulations LOS26, LOS13, and LOS27. All scenarios showed comparable matric suction over time. The results indicate that the long-term variation in matric suction is insensitive to the change in extreme precipitation quantile.

Figure 8. Predicted Time Histories of Mid-Slope Matric Suction at Depth 1 M from the Slope Surface for Climate Scenarios 26, 13 and 29

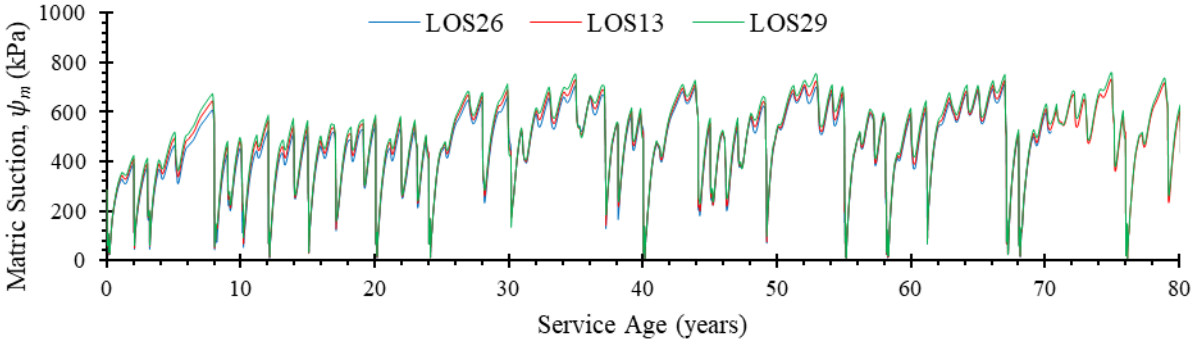

Figure 9 presents the time histories of the predicted mid-slope outward displacement at the slope surface for simulations LOS26, LOS13, and LOS29. It was observed that outward displacement increased with increasing extreme precipitation quantile. This increase grew further over time as more extreme events took place and irrecoverable outward displacements accumulated. The mid-slope outward displacement of the LOS13 simulation (+7% change in extreme precipitation quantile) was predicted to be approximately 116% higher than that of the LOS26 simulation (0% change in precipitation mean). The mid-slope outward displacement of the LOS29 simulation (+14% change in extreme precipitation quantile) was predicted to be approximately 198% higher than that of the LOS26 simulation (0% change in precipitation mean). These results indicate that long-term irrecoverable slope deformation increases significantly with increasing the extreme event precipitation quantile, even when the annual average precipitation remains unchanged.

Figure 9. Predicted Time Histories of Mid-Slope Outward Displacement at the Slope Surface for Climate Scenarios 26, 13 and 29

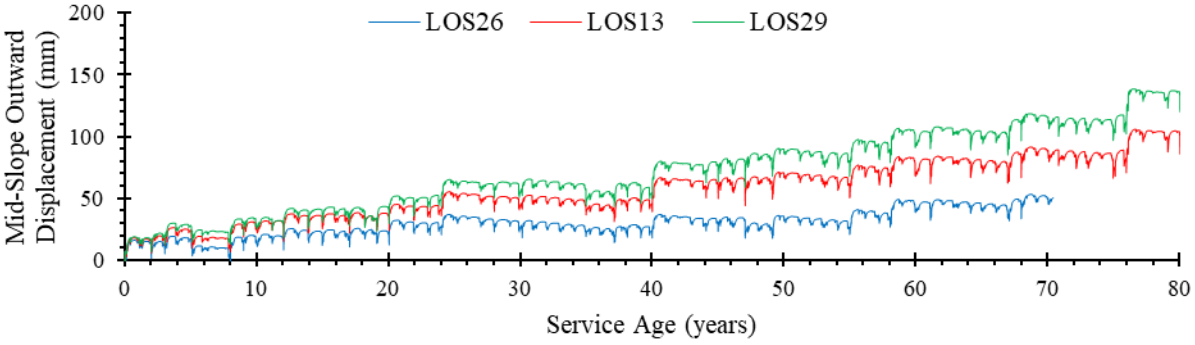

Figure 10 presents the time histories of the predicted mid-slope vertical displacement at the slope surface for simulations LOS26, LOS13, and LOS29. Like the outward displacement, it was observed that vertical displacement (swelling) increased with increasing extreme precipitation quantile. This increase grew further over time as more extreme events took place and irrecoverable vertical displacements accumulated. The mid-slope vertical displacement of the LOS13 simulation (+7% change in extreme precipitation quantile) was predicted to be approximately 51% higher than that of the LOS26 simulation (0% change in precipitation mean). The mid-slope vertical displacement of the LOS29 simulation (+14% change in extreme precipitation quantile) was predicted to be approximately 96% higher than that of the LOS26 simulation (0% change in precipitation mean). These results indicate that long-term irrecoverable slope swelling increases significantly with increasing the extreme event precipitation quantile, even when the annual average precipitation remains unchanged.

Figure 10. Predicted Time Histories of Mid-Slope Vertical Displacement at the Slope Surface for Climate Scenarios 26, 13 and 29

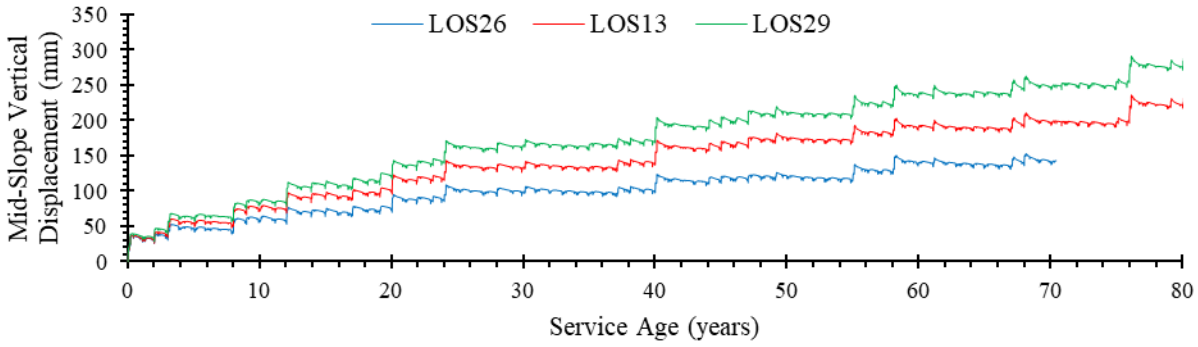

4.3 Effect of Slope Inclination

To evaluate the effect of slope inclination on the sensitivity of the long-term performance of clay embankments to average annual precipitation, numerical simulations were conducted on embankment models with side slopes of 3.0:1, 2.0:1, and 1.5:1 (run to rise) under climate scenarios 1 (baseline), 25, 26, and 27. Table 5 summarizes the parameters of the simulations discussed in this section.

Table 5. Summary of the Long-Term Simulations Conducted to Evaluate the Effect of Slope Inclination

Climate Scenario	Change in Incremental Temperature (°C)	% Change in Extreme Precipitation Quantile	% Change in Precipitation Mean	Side Slope	Soil Type
01	0	0	0	3.0:1	CH
25	+3		−12.5		
26	+3		0		
27	+3		+12.5		
01	0	0	0	2.0:1	CH
25	+3		−12.5		
26	+3		0		
27	+3		+12.5		
01	0	0	0	1.5:1	CH
25	+3		−12.5		
26	+3		0		
27	+3		+12.5		

Figure 11 presents the time histories of the predicted mid-slope matric suction at depth 1 m for simulations LOS01, LOS25, LOS26, and LOS27 of CH embankments with side slopes 3.0:1, 2.0:1, and 1.5:1 (run to rise). When comparing the numerical predictions, it was observed that matric suction increases with decreasing slope steepness. The effect of the various climate scenarios on the embankments with various side slopes was consistent with that observed in embankments with 3.0:1 side slopes discussed earlier. As expected, steeper slopes sustained more damage over time than milder slopes leading to earlier failures. Embankments with side slopes 1.5:1 were predicted to collapse at approximately 24 years under climate scenario 27 and at 40 years under climate scenarios 25 and 26. No failures were observed in the embankments with side slopes 3.0:1 and 2.0:1 for the studied duration of 80 years.

Figure 11. Predicted Time Histories of Mid-Slope Matric Suction at Depth 1 M from the Slope Surface for Climate Scenarios 1, 25, 26, and 27: (a) in CH Embankments with Side Slopes 3.0:1; (b) CH Embankments with Side Slopes 2.0:1; and (c) in CH Embankments with Side Slopes 1.5:1

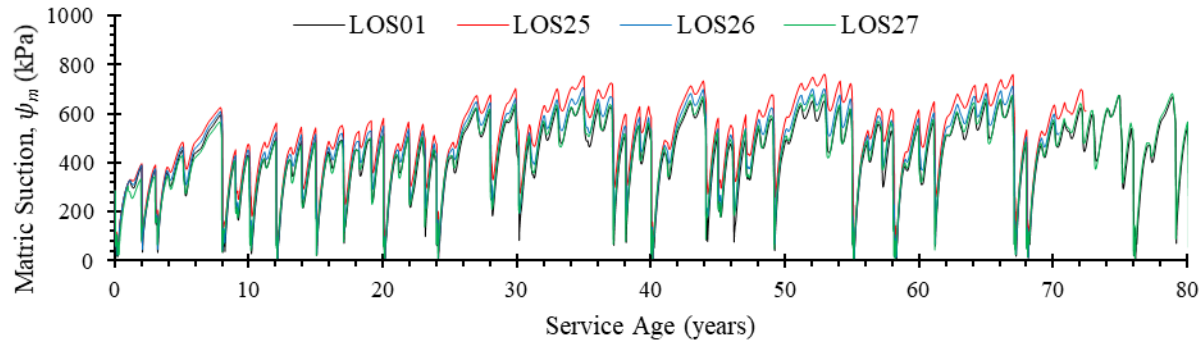

(a)

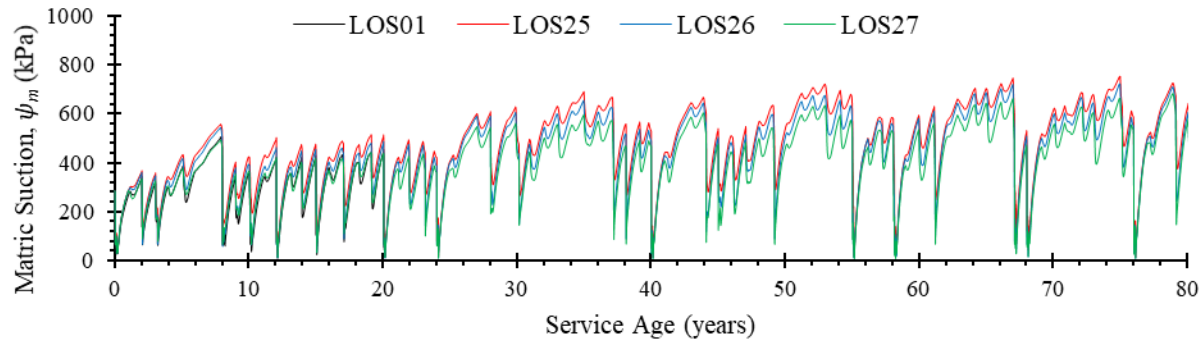

(b)

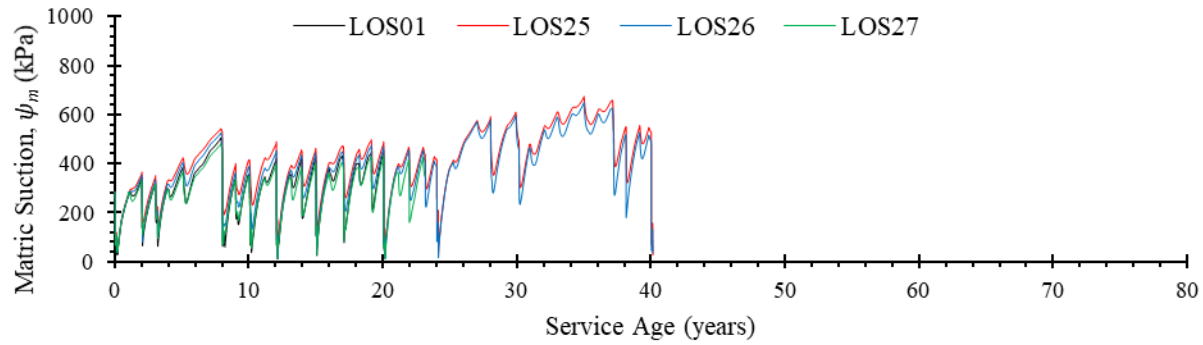

(c)

Figure 12 presents the time histories of the predicted mid-slope outward displacement at the slope surface for simulations LOS01, LOS25, LOS26, and LOS27 of CH embankments with side slopes 3.0:1, 2.0:1, and 1.5:1 (run to rise). As expected, it was observed that outward displacements increased with increasing slope steepness under the various climate scenarios.

Figure 12. Predicted Time Histories of Mid-Slope Outward Displacement at the Slope Surface for Climate Scenarios 1, 25, 26, and 27: (a) in CH Embankments with Side Slopes 3.0:1; (b) CH Embankments with Side Slopes 2.0:1; and (c) in CH Embankments with Side Slopes 1.5:1

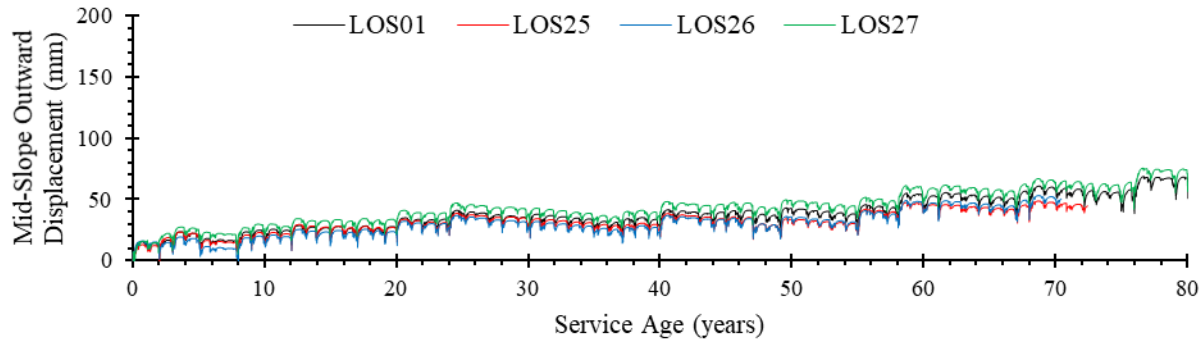

(a)

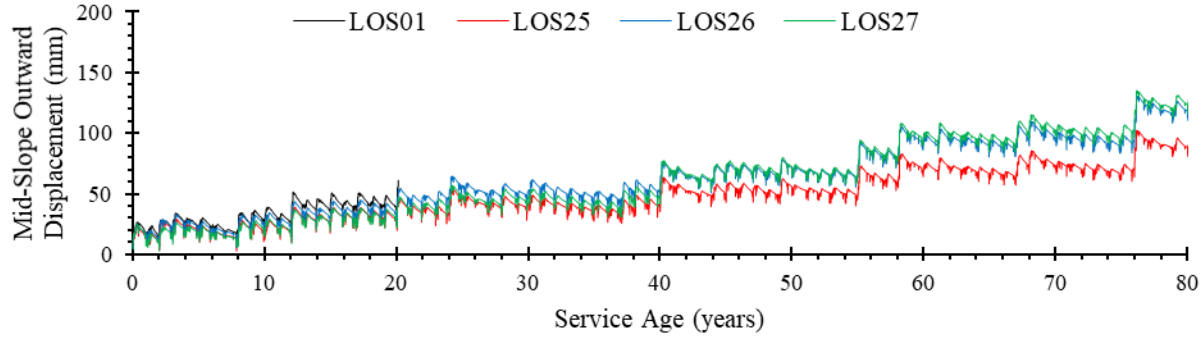

(b)

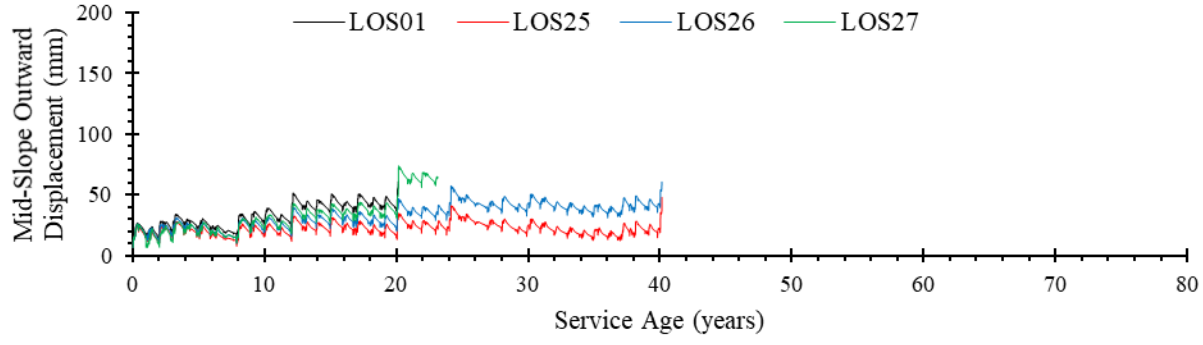

(c)

Figure 13 presents the time histories of the predicted mid-slope vertical displacement at the slope surface for simulations LOS01, LOS25, LOS26, and LOS27 of CH embankments with side slopes 3.0:1, 2.0:1, and 1.5:1 (run to rise). It was observed that vertical displacements (swelling) increased with decreasing slope steepness under the various climate scenarios. These results indicate that milder slopes are more prone to increased irrecoverable swelling over time.

Figure 13. Predicted Time Histories of Mid-Slope Vertical Displacement at the Slope Surface for Climate Scenarios 1, 25, 26, and 27: (a) in CH Embankments with Side Slopes 3.0:1; (b) CH Embankments with Side Slopes 2.0:1; and (c) in CH Embankments with Side Slopes 1.5:1

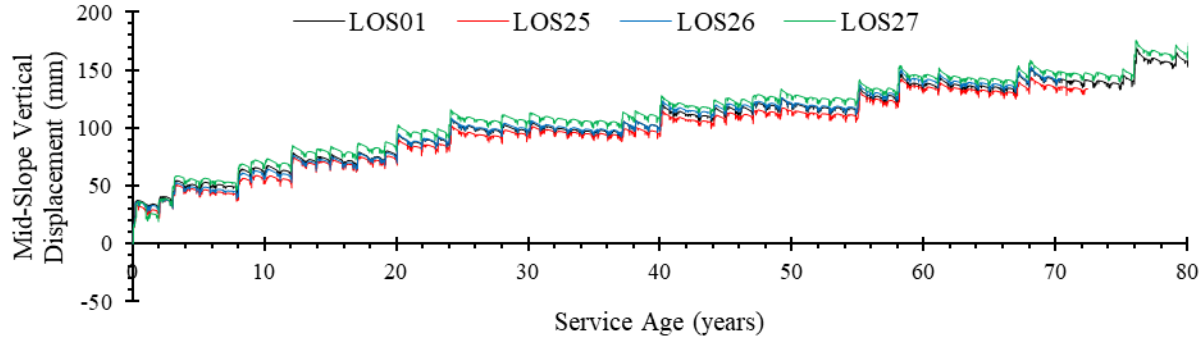

(a)

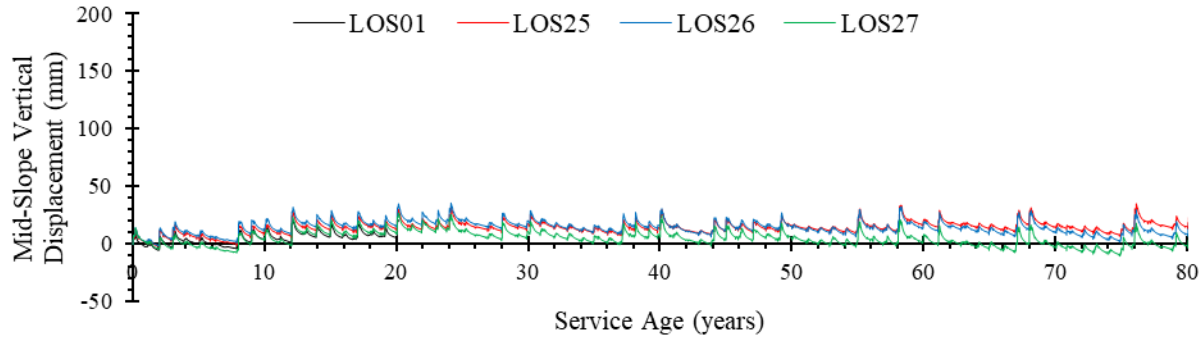

(b)

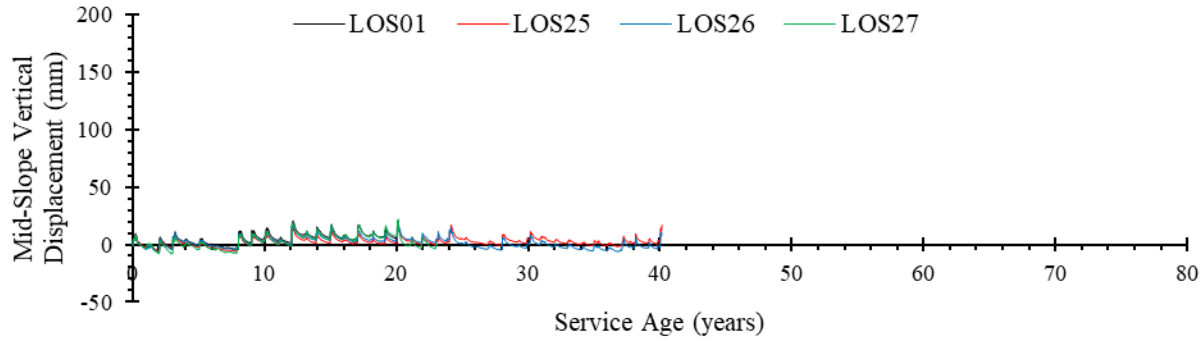

(c)

4.4 Effect of Soil Type

To evaluate the effect of soil plasticity on the sensitivity of the long-term performance of clay embankments to average annual precipitation, numerical simulations were conducted on embankment models with soil parameters representative of CH and CL clays under climate scenarios 1 (baseline), 25, 26, and 27. Table 6 summarizes the parameters of the simulations discussed in this section.

Table 6. Summary of the Long-Term Simulations Conducted to Evaluate the Effect of Soil Type

Climate Scenario	Change in Incremental Temperature (°C)	% Change in Extreme Precipitation Quantile	% Change in Precipitation Mean	Side Slope	Soil Type
01	0	0	0	3.0:1	CH
25	+3		−12.5		
26	+3		0		
27	+3		+12.5		
01	0	0	0	3.0:1	CL
25	+3		−12.5		
26	+3		0		
27	+3		+12.5		

Figure 14 presents the time histories of the predicted mid-slope matric suction at depth 1 m for simulations LOS01, LOS25, LOS26, and LOS27 of CL and CH embankments. When comparing the numerical predictions, larger fluctuations in matric suction were observed in CH embankments than in CL embankments. During wet seasons, the matric suction in CH embankments reduced to near zero, whereas CL embankments maintained adequate matric suction. This suggests that CH embankments are more sensitive to seasonal wet-dry cycles than CL embankments.

Figure 14. Predicted Time Histories of Mid-Slope Matric Suction at Depth 1 M from the Slope Surface for Climate Scenarios 1, 25, 26, and 27: (a) in CH Embankments with Side Slopes 3.0:1; and (b) CL Embankments with Side Slopes 3.0:1

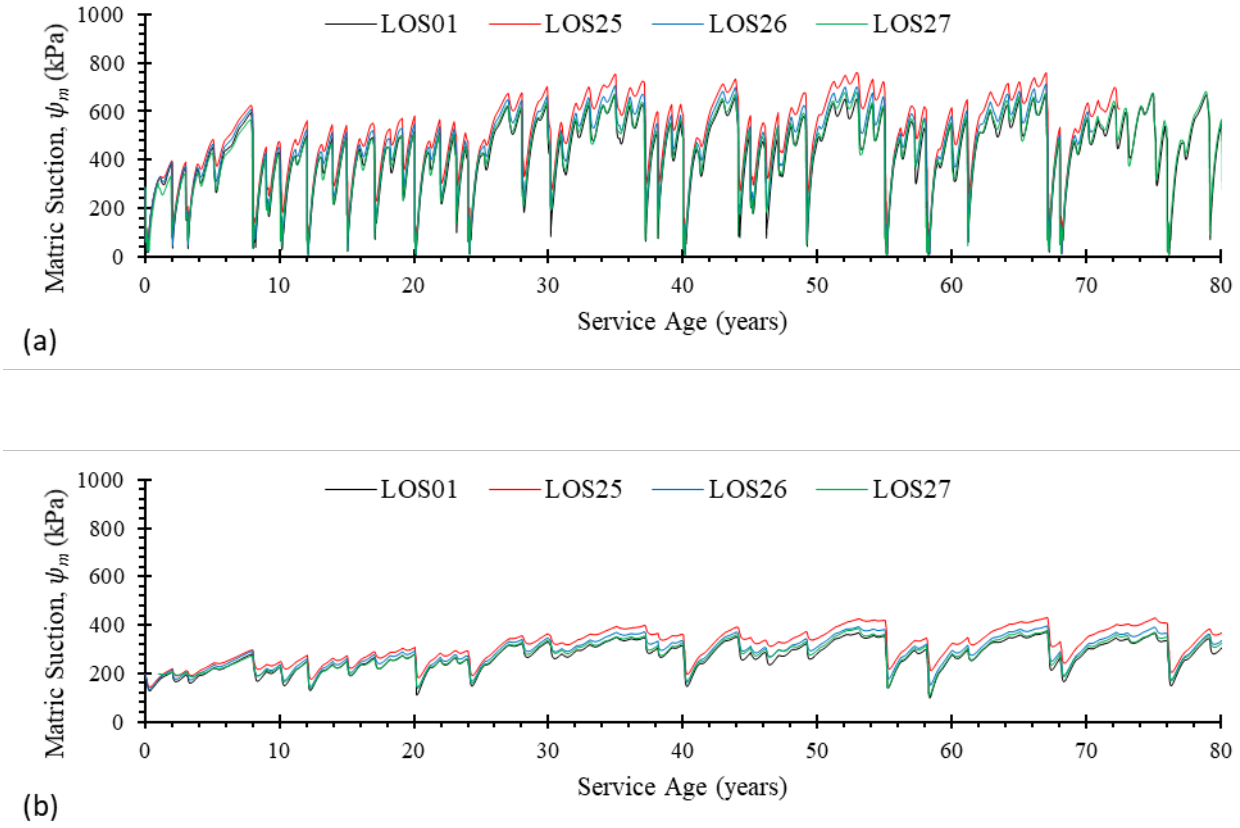

Figure 15 presents the time histories of the predicted mid-slope outward displacement at the slope surface for simulations LOS01, LOS25, LOS26, and LOS27 of CL and CH embankments. When comparing the numerical predictions, larger outward displacements were observed in CH embankments than in CL embankments. The outward displacements in CH embankments increased over time, exhibiting a plastic ratcheting pattern, whereas those in CL embankments fluctuated with seasonal wet-dry cycles and did not show significant accumulation over time. This indicates that CH embankments are more likely to experience long-term irrecoverable deformation under seasonal wetting and drying than CL embankments.

Figure 15. Predicted Time Histories of Mid-Slope Outward Displacement at the Slope Surface for Climate Scenarios 1, 25, 26, and 27: (a) in CH Embankments with Side Slopes 3.0:1; and (b) CL Embankments with Side Slopes 3.0:1

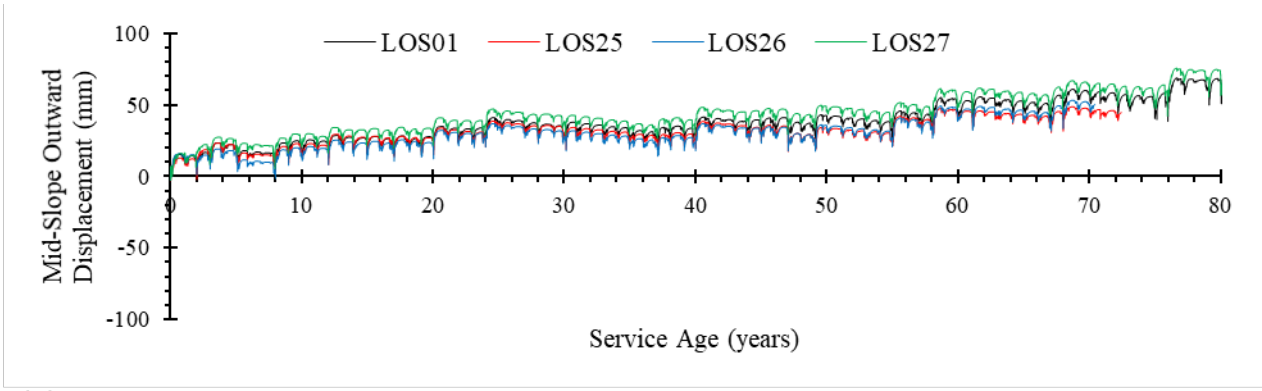

(a)

(b)

Figure 16 presents the time histories of the predicted mid-slope vertical displacement at the slope surface for simulations LOS01, LOS25, LOS26, and LOS27 of CL and CH embankments. Both CH and CL embankments exhibited an increasing irrecoverable swelling over time. The effect of the various climate scenarios on CL embankments is consistent with that observed in the CH embankments discussed earlier.

Figure 16. Predicted Time Histories of Mid-Slope Vertical Displacement at the Slope Surface for Climate Scenarios 1, 25, 26, and 27: (a) in CH Embankments with Side Slopes 3.0:1; and (b) CL Embankments with Side Slopes 3.0:1

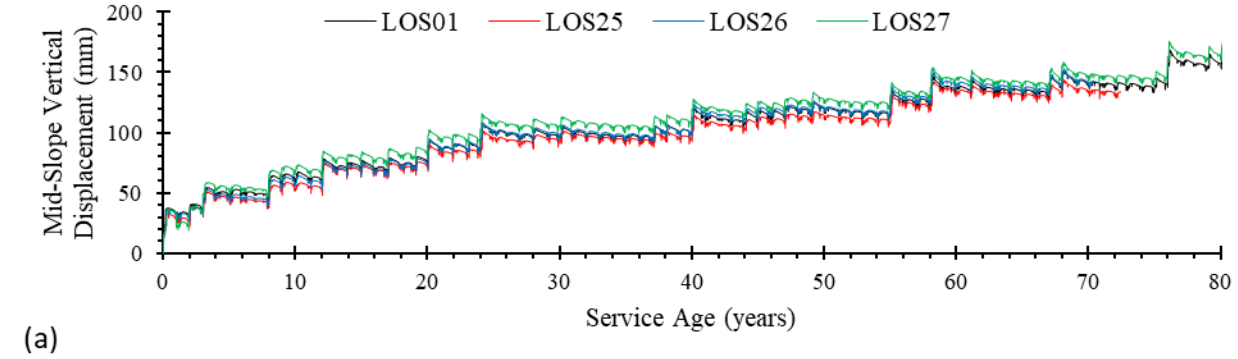

(a)

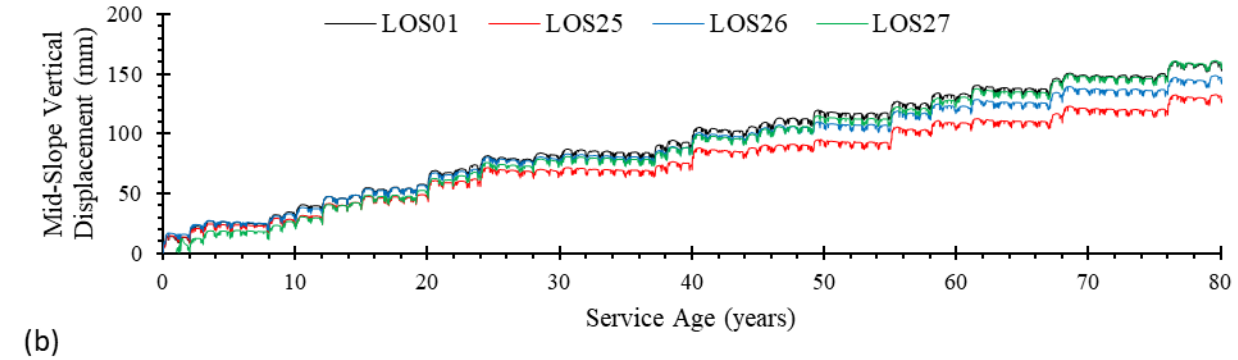

(b)

5. Short-Term Performance of Earth Embankments under Perturbed Extreme Events

A parametric evaluation was conducted to evaluate the effect of extreme precipitation events brought about by perturbed future climate scenarios on the hydromechanical response of clay embankments to these extreme events. The parametric evaluation involved studying the effect of the extreme event precipitation intensity and duration, the effect of slope inclination, and the effect of soil type. The evaluation involved exemplary embankments constructed from high plasticity and low plasticity clays, with side slopes of 3.0:1, 2.0:1, and 1.5:1 (run to rise). The baseline case was selected to be a high plasticity clay (CH) embankment 6 m in height with side slopes 3.0:1 (see Morsy & Varela, 2025). The simulations were performed under 1-day, 3-day, and 7-day extreme precipitation events with a 100-year return period (i.e., events with 1% annual exceedance probability).

Embankment models were subjected to 100-year return period extreme events of durations 1, 3, and 7 days (and corresponding intensities). Simulations were given IDs that denote their geographical location, climate scenario, and extreme event duration. For example, an embankment constructed in Los Angeles and subjected to a 3-day extreme event induced by climate scenario 26 is given an ID of LOS26_D3. Numerical predictions of volumetric water content, matric suction, and surface displacements were curated at three slope locations: 25% *H* above slope toe, 50% *H* above slope toe (mid-slope), and 75% *H* above slope toe; *H* is the slope height.

5.1 Effect of Future Climate Scenarios

To evaluate the effect of future climate scenarios on the short-term performance of clay embankments, numerical simulations were conducted on embankment models with soil parameters representative of CH and CL clays and with side slopes 3.0:1 (run to rise). The models were subjected to climate scenarios 26, 13, and 29, which involve a change in future extreme precipitation quantile of 0%, +7%, and +14%, respectively. These three scenarios involved an incremental increase in future temperature of +3°C and a change in average annual precipitation of 0%. Table 7 summarizes the parameters of the simulations discussed in this section.

Since climate scenario 26 had the same precipitation data as the baseline climate scenario 1 (0% change in annual precipitation average and extreme precipitation quantile), the numerical simulations for both scenarios (LOS01 and LOS26) were identical for short-term extreme precipitation events. Even though LOS26 has a +3°C change in incremental temperature, the numerical simulations of short-term extreme events conducted in this study did not consider the evapotranspiration that may take place during such events. Accordingly, climate scenario 26 was treated as the baseline case (equivalent to climate scenario 1) for short-term performance under extreme events.

Table 7. Summary of the Short-Term Simulations Conducted to Evaluate the Effect of Climate Scenarios

Climate Scenario	Duration (days)	Change in Incremental Temperature (°C)	% Change in Extreme Precipitation Quantile	% Change in Precipitation Mean	Side Slope	Soil Type
26 (baseline)	7	+3	0	0	3.0:1	CH
13			+7			
29			+14			
26 (baseline)	7	+3	0	0	3.0:1	CL
13			+7			
29			+14			

Figure 17 presents the predicted volumetric water content at a depth of 0.5 m for the CH and CL embankment models. The models were subjected to the 7-day precipitation events of climate scenarios LOS26, LOS13, and LOS29. The figure presents the predicted volumetric water content at three slope locations: 0.25*H*, 0.50*H*, and 0.75*H* above slope toe.

For CH embankments, shown in Figure 17a, it was observed that the near-surface volumetric water content would likely increase (wetter slopes) with increasing the change in future rainfall intensity. In these simulations, the moisture at the toe of the slope increased first (around day 2), followed by the crest (around day 3), and the middle slope (around day 4). Among the three scenarios, LOS29 caused the slope to saturate the fastest, followed by LOS13, and LOS01. Near the toe of the slope, the predicted volumetric water content increased by about 5% under LOS13 (+7% change in extreme precipitation quantile) and by 7% under LOS29 (+14% change in extreme precipitation quantile) as compared to LOS26 (baseline case; no change in extreme precipitation quantile). The crest and mid-slope locations showed similar trends but with slightly smaller and delayed increases in saturation. The results indicate that future extreme rainfall events induced by perturbed future climate scenarios are projected to increase the saturation of CH embankments, which may lead to an increased probability in rainfall-induced slope failures.

For CL embankments, shown in Figure 17b, the effect of future climate was rather small, resulting in ~1–2% increases in water content under future climate scenarios LOS29 and LOS13 as compared to the baseline climate scenario LOS26. This suggests that CL embankments are much less vulnerable to future extreme rainfall events brought about by perturbed future climate scenarios than CH embankments.

Figure 17. Volumetric Water Content at 0.5 M Depth Over 7 Days at 0.25H, 0.5H and 0.75H for Climate Scenarios 1, 13, and 29: (a) in CH Embankments with 3.0:1 Side Slope; and (b) in CL Embankments with 3.0:1 Side Slope

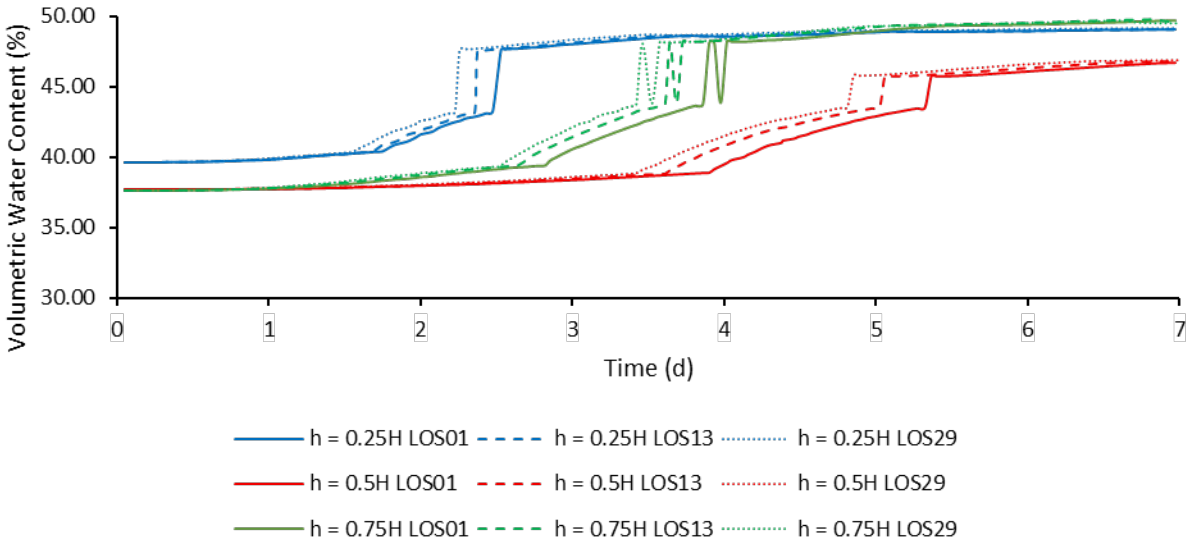

(a)

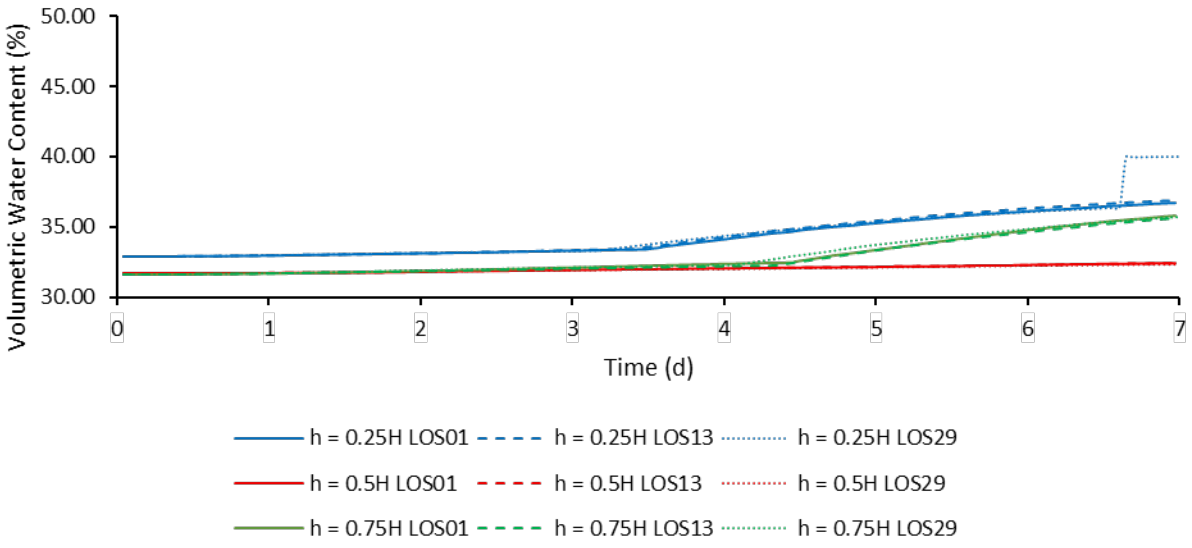

(b)

Figure 18 presents the predicted matric suction at a depth of 0.5 m for the CH and CL embankment models. The models were subjected to the 7-day precipitation events of climate scenarios LOS26, LOS13, and LOS29. The figure presents the predicted matric suction at three slope locations: 0.25H, 0.50H, and 0.75H above slope toe.

For CH embankments, shown in Figure 18a, it was observed that the near-surface matric suction would likely decrease (wetter slopes) with increasing rainfall intensity during future extreme events. In these simulations, the toe lost suction the fastest, followed by the crest and the mid-slope. The decline rate in matric suction was observed to be the largest in LOS29 (largest precipitation intensity), reaching near saturation around day 7, followed by LOS13 and LOS26 (lowest precipitation intensity). This rapid decline in matric suction would result in a loss in shear strength and an increase in potential failure in CH soil under future climate scenarios.

For CL embankments, shown in Figure 18b, similar matric suction trends to those of CH embankments were observed. CL embankments retained more matric suction under extreme events (precipitation intensity and duration) compared to CH embankments. This observation suggests that CL embankments are more resilient to strength loss (due to loss in matric suction) during extreme events than CH embankments. It is notable that the hydraulic characteristics of CH and CL soils used in this study were identical except for the air-entry matric suction (higher in CH than in CL) and porosity (higher in CH than in CL).

Figure 18. Matric Suction at 0.5 M Depth Over 7 Days at 0.25H, 0.5H and 0.75H for Climate Scenarios 1, 13, and 29: (a) in CH Embankments with 3.0:1 Side Slope; and (b) in CL Embankments with 3.0:1 Side Slope

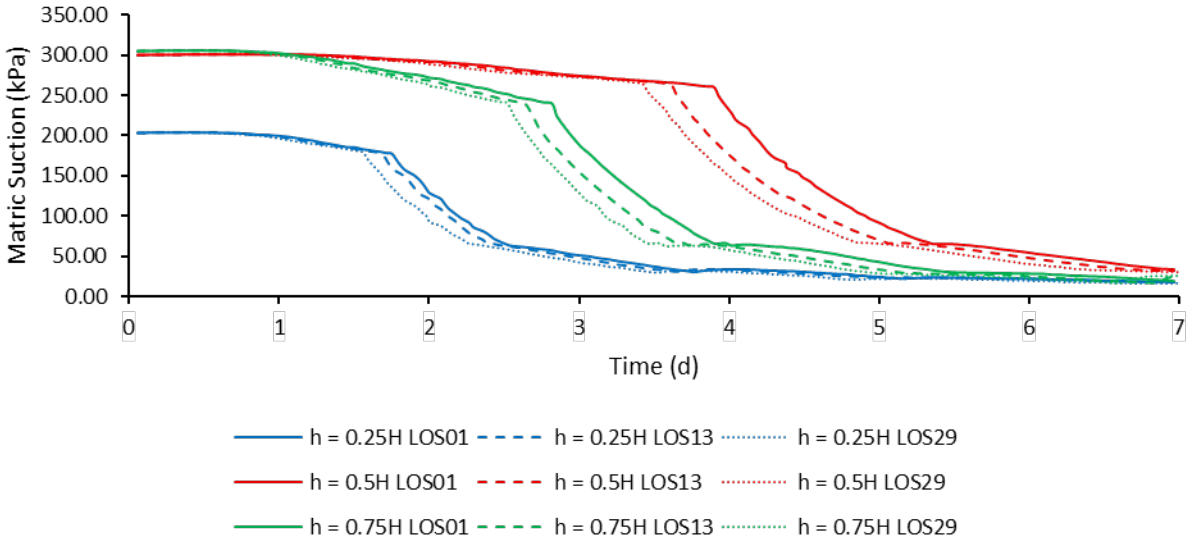

(a)

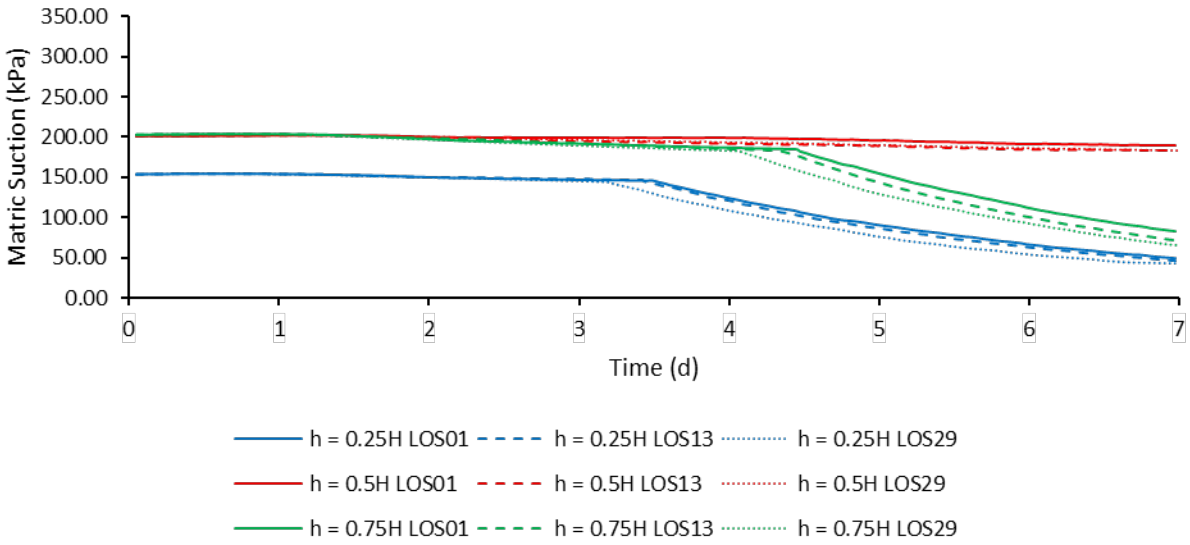

(b)

Figure 19 presents the predicted horizontal surface displacement for the CH and CL embankment models as of the onset of the extreme event. The models were subjected to the 7-day precipitation events of climate scenarios LOS26, LOS13, and LOS29. The figure presents the predicted displacements at three slope locations: 0.25*H*, 0.50*H*, and 0.75*H* above slope toe.

For CH embankments, shown in Figure 19a, it was observed that surface displacement rates were exacerbated as water infiltration advanced below the slope surface, as indicated by the volumetric water content predictions (see Figure 17), especially as infiltration advanced to the 0.5-m depth at day 3. After this point, it was observed that the surface horizontal displacement increased with increasing precipitation intensity. Specifically, LOS29 (highest precipitation intensity) was observed to cause the largest horizontal displacement followed by LOS13 then LOS26 (lowest precipitation intensity) along the entire slope. The horizontal surface displacement at the end of the extreme event LOS29 (after 7 days) was predicted at +2 mm (outward) near the slope toe and at –1 mm (inward) at mid-slope and near the slope crest.

For CL embankments, shown in Figure 19b, the observed displacement trends were similar to those of CH embankments. However, CL embankments did not reach near saturation conditions as CH embankments did (see Figure 17). Therefore, unlike in CH embankments, no tendency to outward displacement was observed in CL embankments during the durations of the studied extreme events.

Figure 19. Horizontal Surface Displacement Over 7 Days at 0.25H, 0.5H and 0.75H for Climate Scenarios 1, 13, and 29: (a) in CH Embankments with 3.0:1 Side Slope; and (b) in CL Embankments with 3.0:1 Side Slope

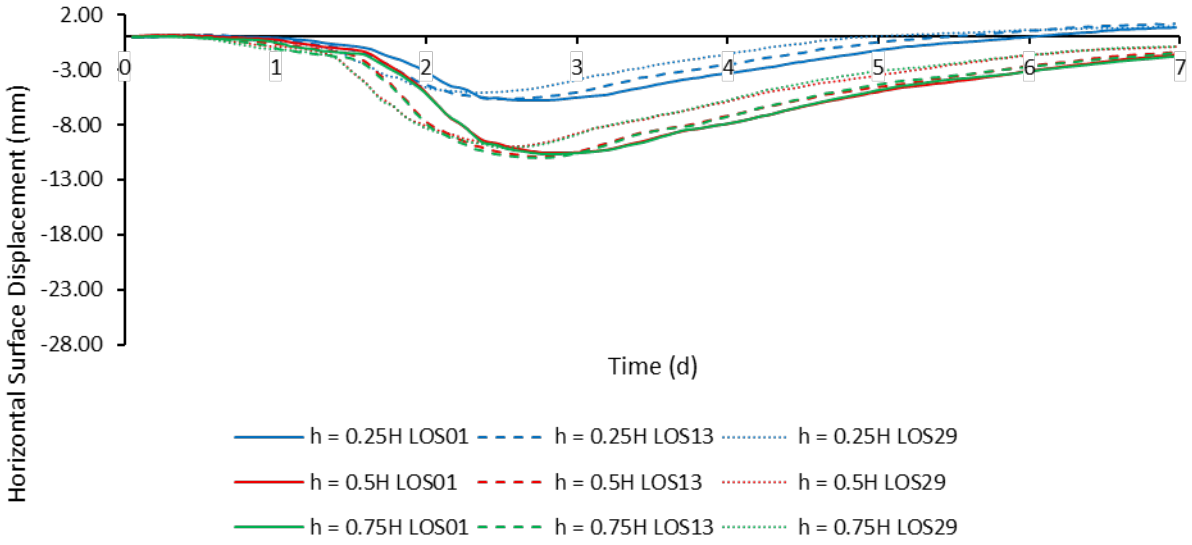

(a)

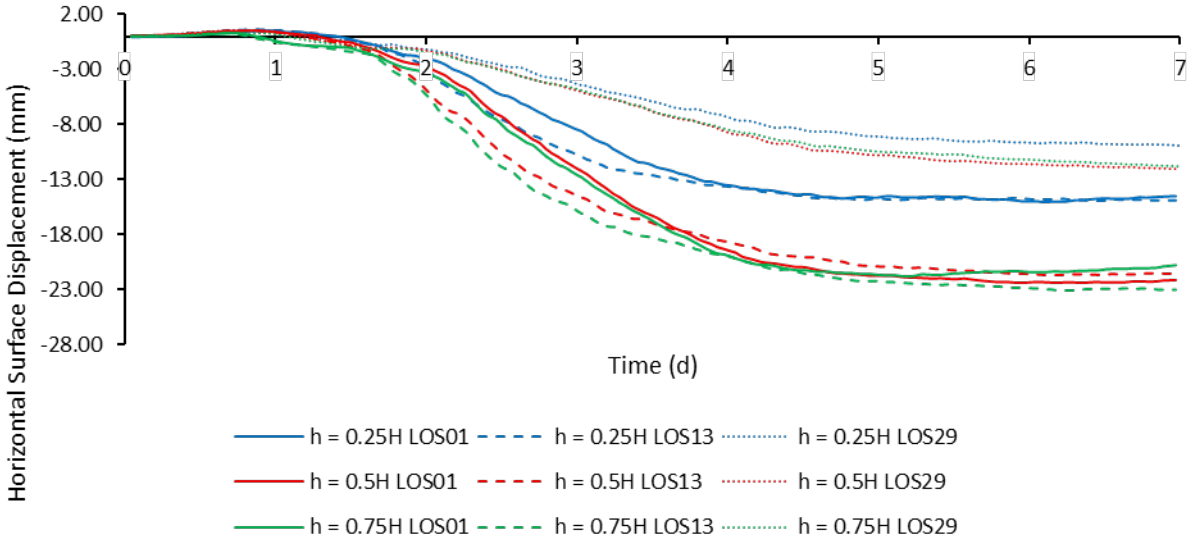

(b)

Figure 20 presents the predicted vertical surface displacement for the CH and CL embankment models as of the onset of the extreme event. The models were subjected to the 7-day precipitation events of climate scenarios LOS26, LOS13, and LOS29. The figure presents the predicted displacements at three slope locations: 0.25H, 0.50H, and 0.75H above slope toe.

For CH embankments, shown in Figure 20a, it was observed that surface vertical displacement (swelling) rates were exacerbated as water infiltration advanced below the slope surface, as indicated by the volumetric water content predictions (see Figure 17), especially as infiltration advanced to the 0.5-m depth at day 3. Predicted vertical displacements increased with increasing event precipitation intensity, where the highest displacement (swelling) was observed in LOS29, followed by LOS13 and LOS26. This displacement pattern is attributable to the swelling of high plasticity clays upon wetting. The vertical surface displacement observed near crest in LOS13 and LOS29 was 3% and 18% higher respectively than that observed in LOS26 (baseline scenario). Similar trends were observed in the vertical displacements at mid-slope and near toe. The results suggest that future extreme precipitation events are likely to exacerbate rainfall-induced swelling in CH embankments, especially in the upper parts of side slopes, increasing the potential of swelling-induced failures.

For CL embankments, shown in Figure 20b, the observed displacement trends were similar to those of CH embankments. However, CL embankments did not reach near saturation conditions as CH embankments did (see Figure 17). Therefore, unlike in CH embankments, no swelling displacements were observed in CL embankments during the duration of the studied extreme events. Nevertheless, CL embankments showed a greater tendency to settle during extreme events than CH embankments.

Figure 20. Vertical Surface Displacement Over 7 Days at 0.25H, 0.5H and 0.75H for Climate Scenarios 1, 13, and 29: (a) in CH Embankments with 3.0:1 Side Slope; and (b) in CL Embankments with 3.0:1 Side Slope

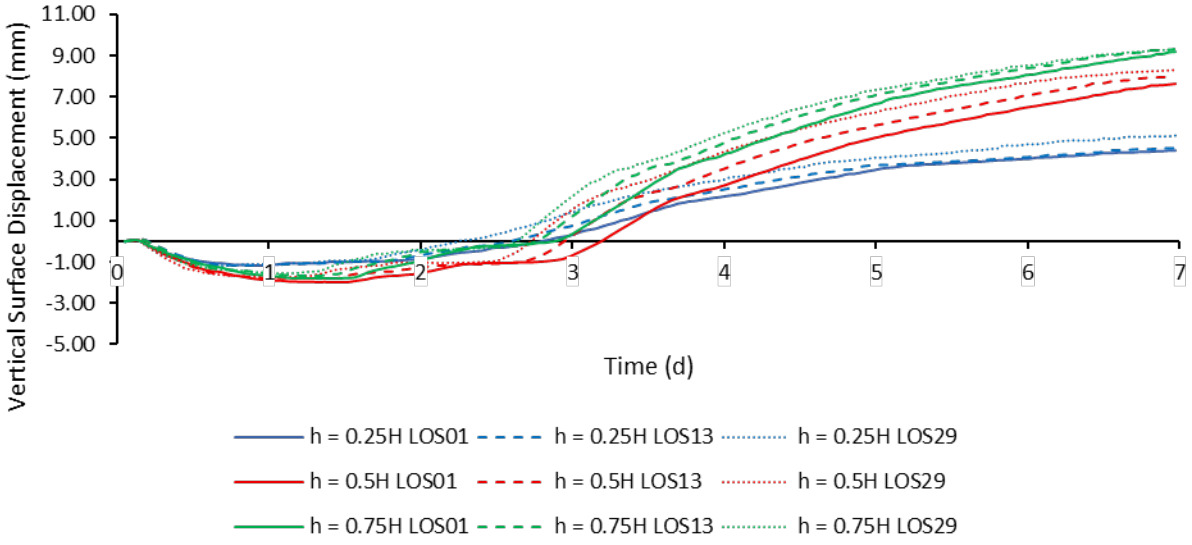

(a)

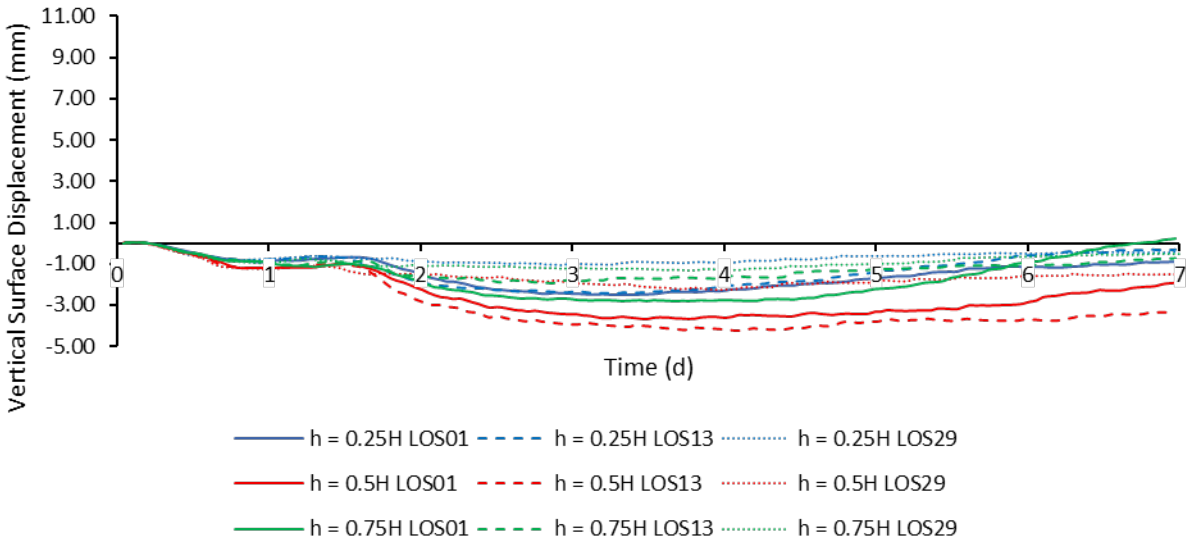

(b)

5.2 Effect of Extreme Event Intensity and Duration

To evaluate the effect of extreme event intensity and duration on the short-term performance of clay embankments, numerical simulations were conducted on embankment models with soil parameters representative of CH and CL clays and with site slopes 3.0:1 (run to rise). The models were subjected to the 1-day, 3-day, and 7-day extreme events induced by climate scenario 29. This climate scenario involved a change in future extreme precipitation quantile of +7%, an incremental increase in future temperature of +3°C, and a change in average annual precipitation of 0%. Precipitation intensities of the extreme events were 27.4 mm/day for the 1-day event, 22.3 mm/day for the 3-day event, and 17.7 mm/day for the 7-day event. Table 8 summarizes the parameters of the simulations discussed in this section.

Table 8. Summary of the Short-Term Simulations Conducted to Evaluate the Effect of Extreme Event Intensity and Duration

Climate Scenario	Duration (days)	Change in Incremental Temperature (°C)	% Change in Extreme Precipitation Quantile	% Change in Precipitation Mean	Side Slope	Soil Type
29	1	+3	+14	0	3.0:1	CH
	3					
	7					
29	1	+3	+14	0	3.0:1	CL
	3					
	7					

Figure 21 presents the predicted volumetric water content at a depth of 0.5 m for the CH and CL embankment models. The models were subjected to the 1-day, 3-day, and 7-day precipitation events of climate scenario LOS29. The figure presents the predicted volumetric water content at three slope locations: 0.25*H*, 0.50*H*, and 0.75*H* above slope toe.

For CH embankments, shown in Figure 21a, it was observed, as expected, that volumetric water content increased with increasing the extreme event duration. The water content increased near the slope toe first (around day 1) followed by the slope crest and mid-slope. The 3-day event (LOS29_D3) caused water to rise earlier than the 7-day event (LOS29_D7) at all slope zones. This was because the 3-day event had a slightly higher precipitation intensity than that of the 7-day event.

For CL embankments, shown in Figure 21b, a smaller increase in water content was observed in comparison to CH embankments. It could be inferred from the results that CH embankments are more sensitive to both precipitation intensity and duration than CL embankments.

Figure 21. Volumetric Water Content at 0.5 M Depth at 0.25H, 0.5H and 0.75H for Extreme Event Durations 1, 3, and 7 Days and Climate Scenario 29: (a) in CH Embankments with 3.0:1 Side Slope; and (b) in CL Embankments with 3.0:1 Side Slope

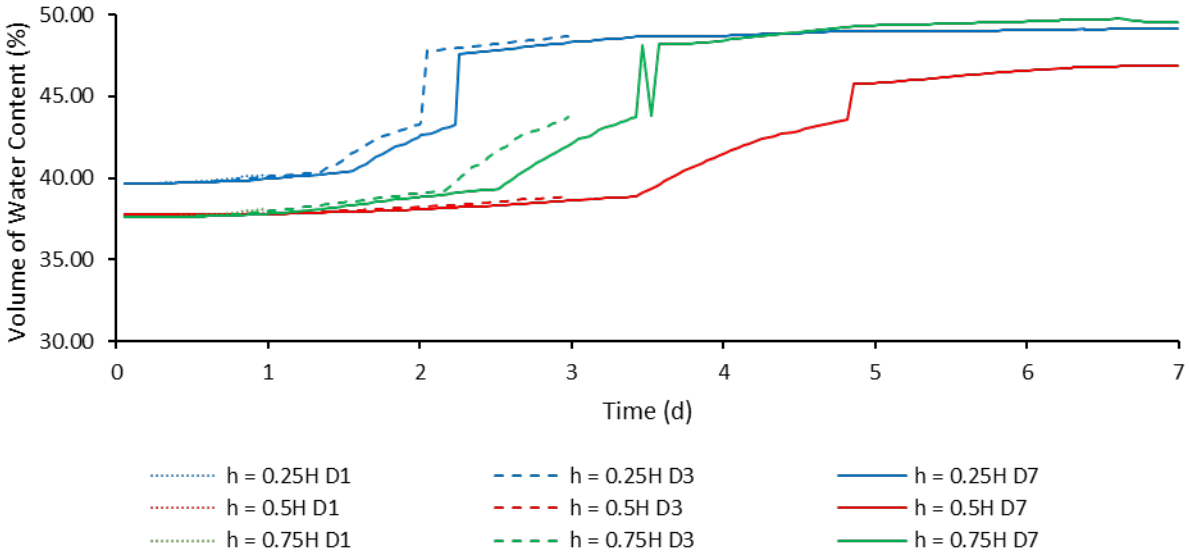

(a)

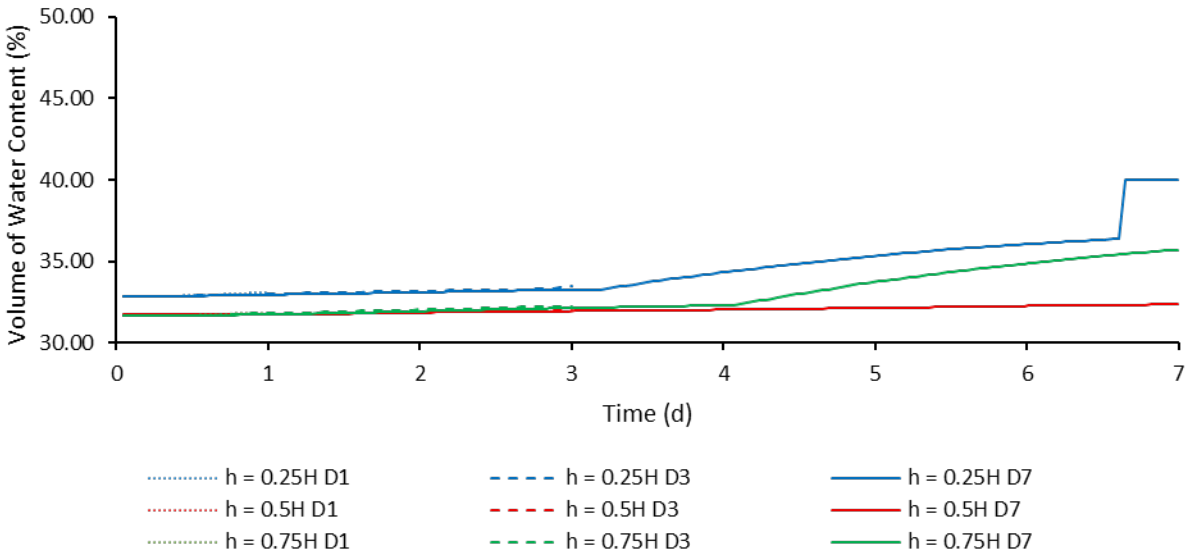

(b)

Figure 22 presents the predicted matric suction at a depth of 0.5 m for the CH and CL embankment models. The models were subjected to the 1-day, 3-day, and 7-day precipitation events of climate scenario LOS29. The figure presents the predicted matric suction at three slope locations: 0.25*H*, 0.50*H*, and 0.75*H* above slope toe.

For CH embankments, shown in Figure 22a, it was observed that the matric suction declined during extreme precipitation events. This decline increased with increasing event duration. It is notable that the time of matric suction drop onset increased with increasing event duration (longer events involve lower precipitation intensity). The results indicate that CH embankments are more sensitive to event duration than event intensity considering extreme events of the same return period.

For CL embankments, shown in Figure 22b, the matric suction patterns were similar to those observed in CH embankments, except that the suction decline in CL embankments was delayed and lower compared to CH embankments. The 1-day event (LOS29_D1) was short enough not to cause a change in the matric suction at 0.5-m depth during the event duration. The 7-day event (LOS29_D7) caused a clear drop in matric suction. Overall, similar to CH embankments, CL embankments are more sensitive to event duration than event intensity considering extreme events of the same return period.

Figure 22. Matric Suction at 0.5 M Depth at 0.25H, 0.5H and 0.75H for Extreme Event Durations 1, 3, and 7 Days and Climate Scenario 29: (a) in CH Embankments with 3.0:1 Side Slope; and (b) in CL Embankments with 3.0:1 Side Slope

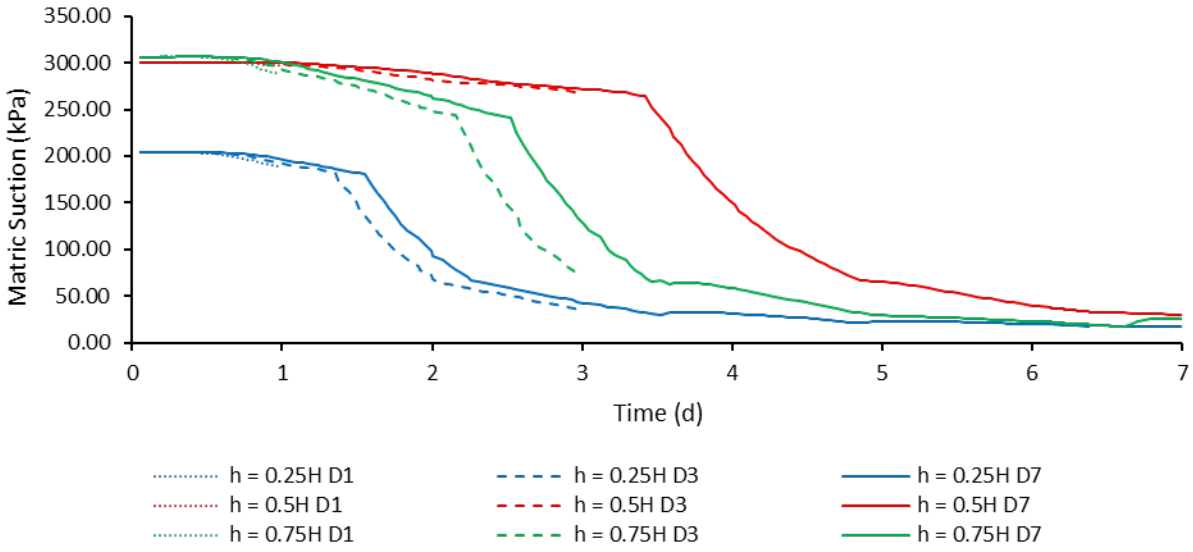

(a)

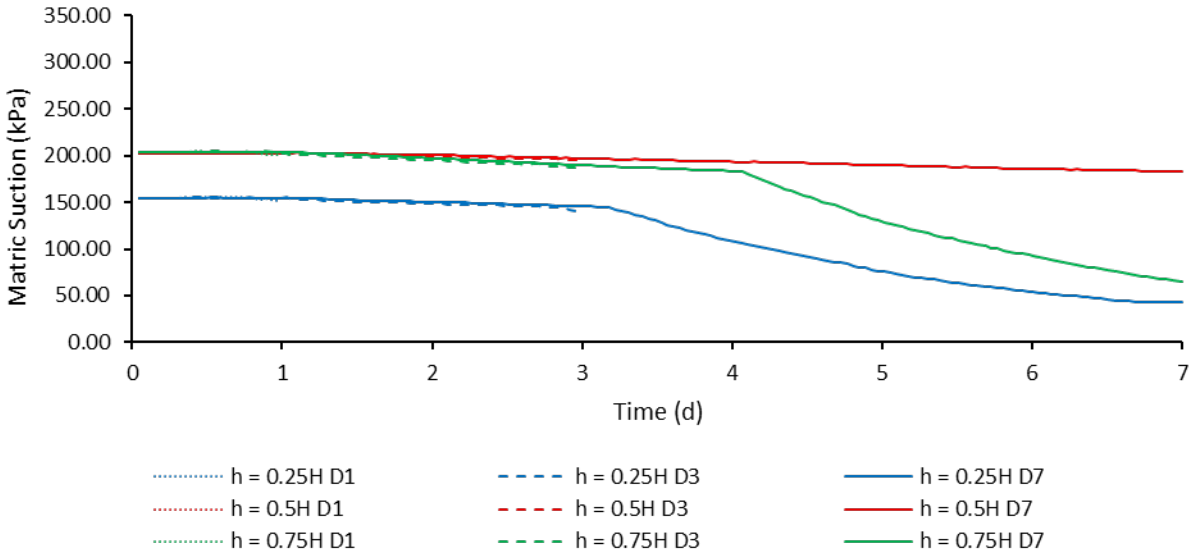

(b)

Figure 23 presents the predicted plastic deviatoric strain (irrecoverable strain) at a depth of 0.5 m for the CH and CL embankment models. The models were subjected to the 1-day, 3-day, and 7-day precipitation events of climate scenario LOS29. The figure presents the predicted plastic deviatoric strain at three slope locations: 0.25*H*, 0.50*H*, and 0.75*H* above slope toe.

For CH embankments, shown in Figure 23a, it was observed that plastic deviatoric strains increased with increasing event duration. Shorter duration events (events with higher precipitation intensity for the same return period) caused plastic strains earlier than longer duration events. Overall, the results indicate that CH embankments are likely to sustain irrecoverable strains by 100-year extreme events that last for more than 2 days.

For CL embankments, shown in Figure 23b, the observed plastic deviatoric strains were insignificant and accumulated after 3 to 4 days. The results suggest that CL embankments are much less susceptible to irrecoverable strains during extreme events in comparison to CH embankments.

Figure 23. Plastic Deviatoric Strain at 0.5 M Depth at 0.25H, 0.5H and 0.75H for Extreme Event Durations 1, 3, and 7 Days and Climate Scenario 29: (a) in CH Embankments with 3.0:1 Side Slope; and (b) in CL Embankments with 3.0:1 Side Slope

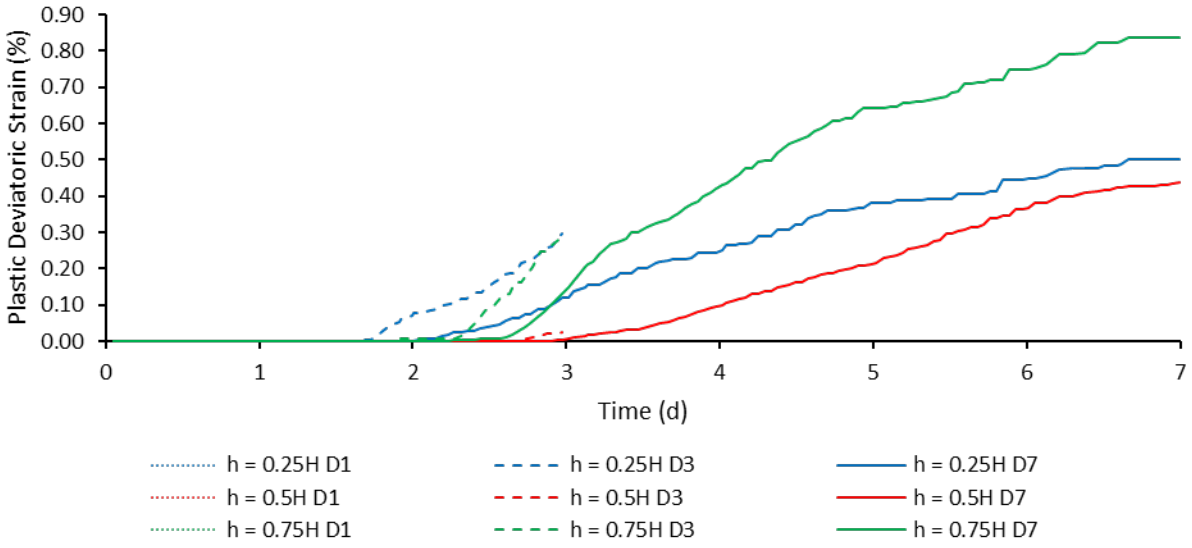

(a)

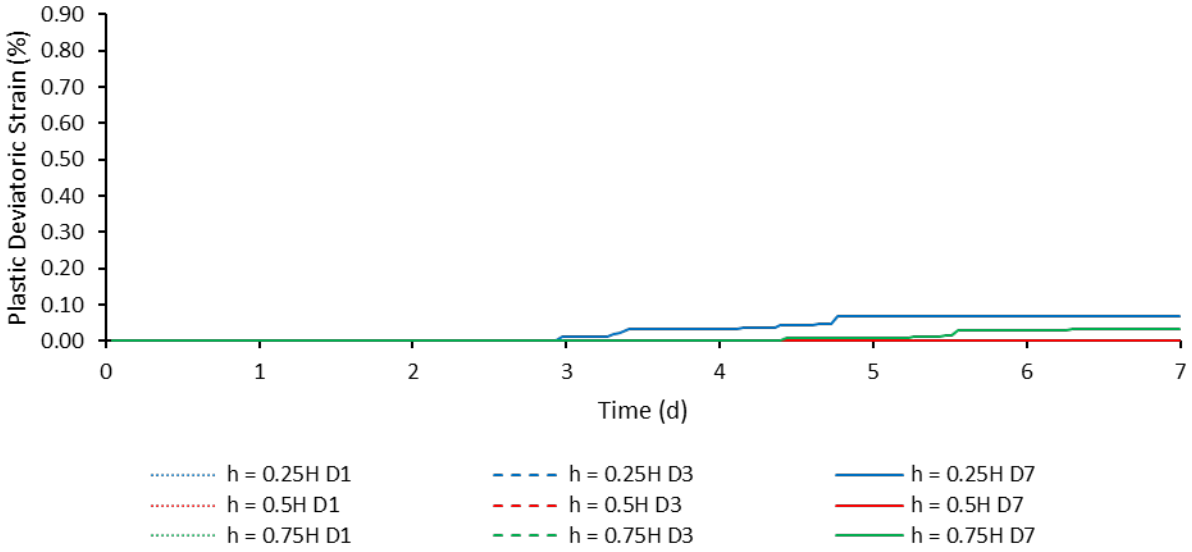

(b)

5.3 Effect of Slope Inclination

To evaluate the effect of slope inclination on the short-term performance of clay embankments during extreme precipitation events, numerical simulations were conducted on embankment models with soil parameters representative of CH and CL clays and with side slopes 3.0:1, 2.0:1, and 1.5:1 (run to rise), subject to climate scenario 13. This climate scenario involved a change in future extreme precipitation quantile of +7%, an incremental increase in future temperature of +3˚C, and a change in average annual precipitation of 0%. Table 9 summarizes the parameters of the simulations discussed in this section.

Table 9. Summary of the Short-Term Simulations Conducted to Evaluate the Effect of Slope Inclination

Climate Scenario	Duration (days)	Change in Incremental Temperature (˚C)	% Change in Extreme Precipitation Quantile	% Change in Precipitation Mean	Side Slope	Soil Type
13	7	+3	+7	0	3.0:1	CH
					2.0:1	
					1.5:1	
13	7	+3	+7	0	3.0:1	CL
					2.0:1	
					1.5:1	

Figure 24 presents the predicted volumetric water content at a depth of 0.5 m for the CH and CL embankment models. Models of side slopes 3.0:1, 2.0:1, and 1.5:1 were subjected to the 7-day precipitation events of climate scenario LOS13. The figure presents the predicted volumetric water content at three slope locations: 0.25H, 0.50H, and 0.75H above slope toe.

For CH embankments, shown in Figure 24a, it was observed that the near-surface volumetric water content increased earlier (earlier wetting; faster infiltration) in steeper slopes (1.5:1) than in milder slopes (3.0:1). For CL embankments, shown in Figure 24b, a similar observation was made where the near-surface volumetric water content increased earlier in steeper slopes than in milder slopes. Overall, the results indicate that steeper slopes tend to wet faster than milder slopes, which makes them more vulnerable to failure even during comparatively short extreme precipitation events.

Figure 24. Volumetric Water Content at 0.5 M Depth Over 7 Days at 0.25H, 0.5H and 0.75H for Side Slopes 1.5:1, 2.0:1, and 3.0:1 and Climate Scenario 13: (a) in CH Embankments; and (b) in CL Embankments

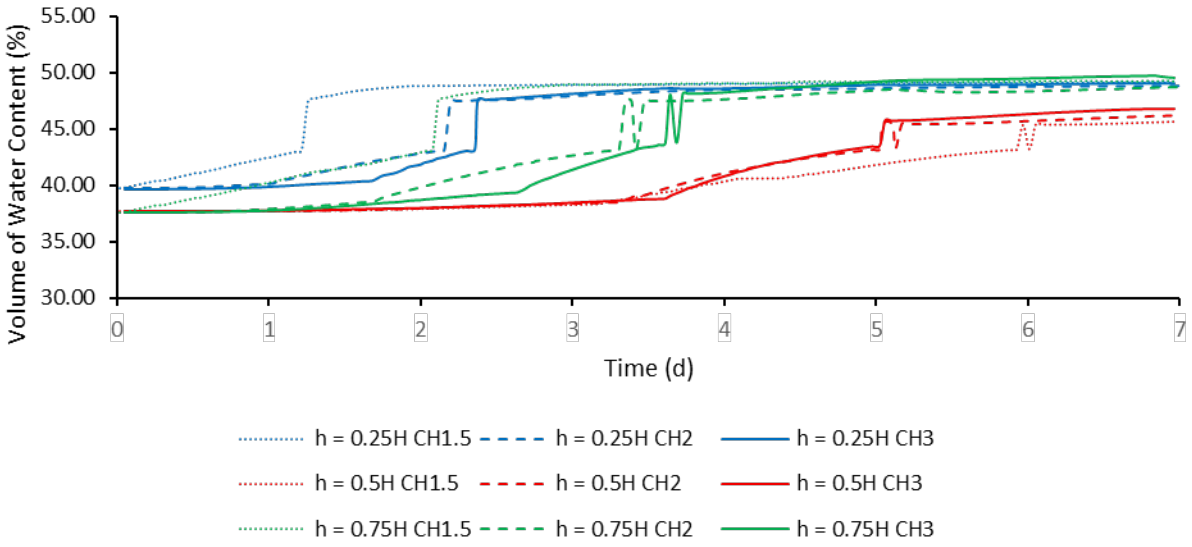

(a)

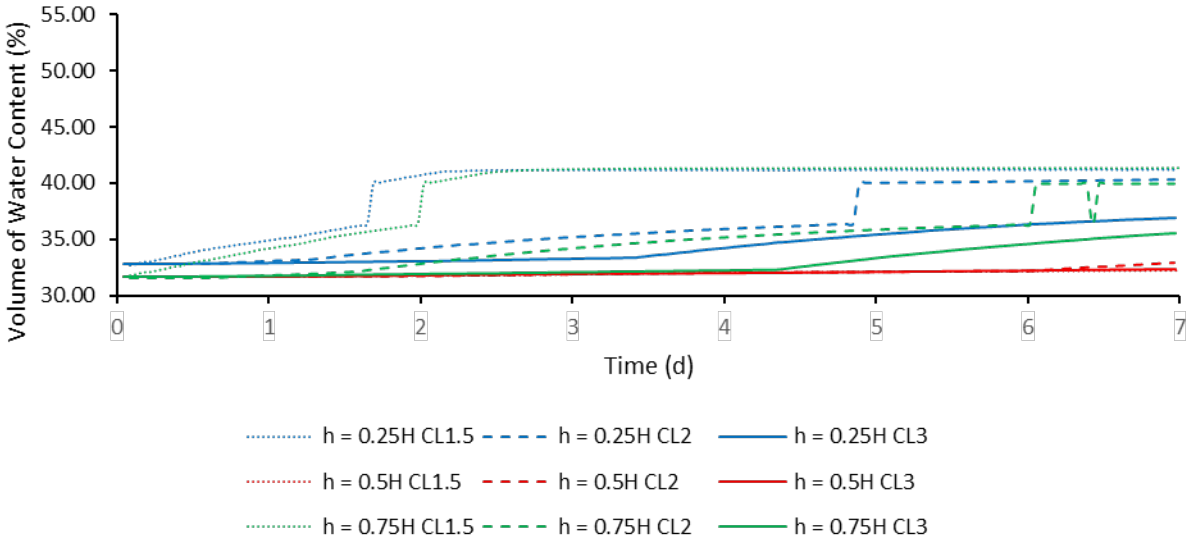

(b)

Figure 25 presents the matric suction at a depth of 0.5 m for the CH and CL embankment models. Models of side slopes 3.0:1, 2.0:1, and 1.5:1 were subjected to the 7-day precipitation events of climate scenario LOS13. The figure presents the predicted matric suction at three slope locations: 0.25*H*, 0.50*H*, and 0.75*H* above slope toe.

For CH embankments, shown in Figure 25a, it was observed that the near-surface matric suction decreased earlier (earlier wetting; faster infiltration) in steeper slopes (1.5:1) than in milder slopes (3.0:1). By the end of the event (7 days), the matric suction diminished as near-surface soil approached saturation. For CL embankments, shown in Figure 25b, a similar observation was made where the near-surface matric suction decreased earlier in steeper slopes than in milder slopes. Overall, the results indicate that steeper slopes tend to wet faster than milder slopes, leading to a rapid loss in matric suction and shear strength, which makes them more vulnerable to failure even during comparatively short extreme precipitation events.

Figure 25. Matric Suction at 0.5 M Depth Over 7 Days at 0.25H, 0.5H and 0.75H for Side Slopes 1.5:1, 2.0:1 and 3.0:1 and Climate Scenario 13: (a) in CH Embankments; and (b) in CL Embankments

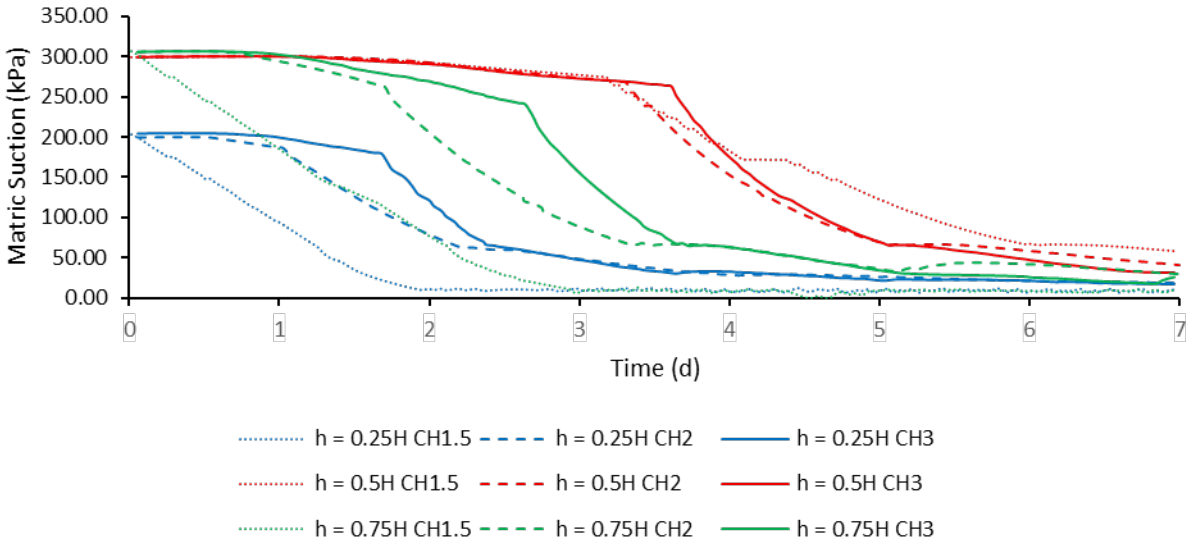

(a)

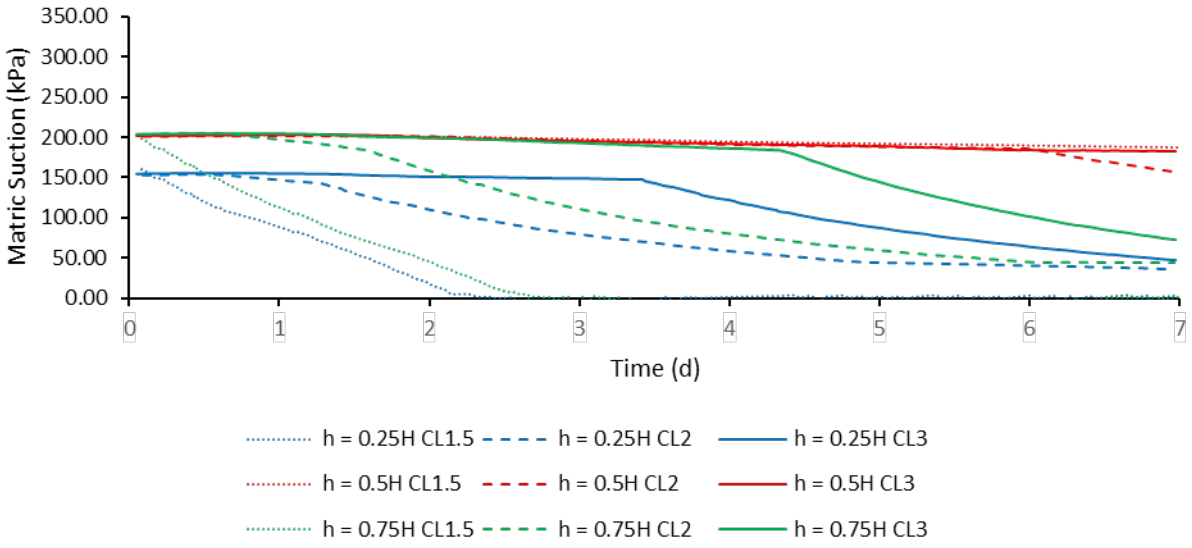

(b)

Figure 26 presents the predicted horizontal surface displacement for the CH and CL embankment models as of the onset of the extreme event. Models of side slopes 3.0:1, 2.0:1, and 1.5:1 were subjected to the 7-day precipitation events of climate scenario LOS13. The figure presents the predicted displacements at three slope locations: 0.25*H*, 0.50*H*, and 0.75*H* above slope toe.

For CH embankments, shown in Figure 26a, a rapid increase in horizontal surface displacement was observed as infiltration progressed to depth 0.5 m. The outward displacement rate increased with increasing slope steepness; the 1.5:1 slope displaced outwards at a higher rate than the 2.1:1 slope than the 3.0:1 slope. This indicates that CH embankments with steeper slopes are more prone to outward displacements during extreme events than milder slopes. Such outward displacements are likely to initiate in CH embankments subject to extreme events longer than 3 days.

For CL embankments, shown in Figure 26b, the observed displacement trends were similar to those of CH embankments. However, CL embankments did not reach near saturation conditions as CH embankments did. Therefore, unlike in CH embankments, no tendency to outward displacement was observed in CL embankments during the duration of the studied extreme events.

Figure 26. Horizontal Surface Displacement Over 7 Days at 0.25H, 0.5H and 0.75H for Side Slopes 1.5:1, 2.0:1 and 3.0:1 and Climate Scenario 13: (a) in CH Embankments; and (b) in CL Embankments

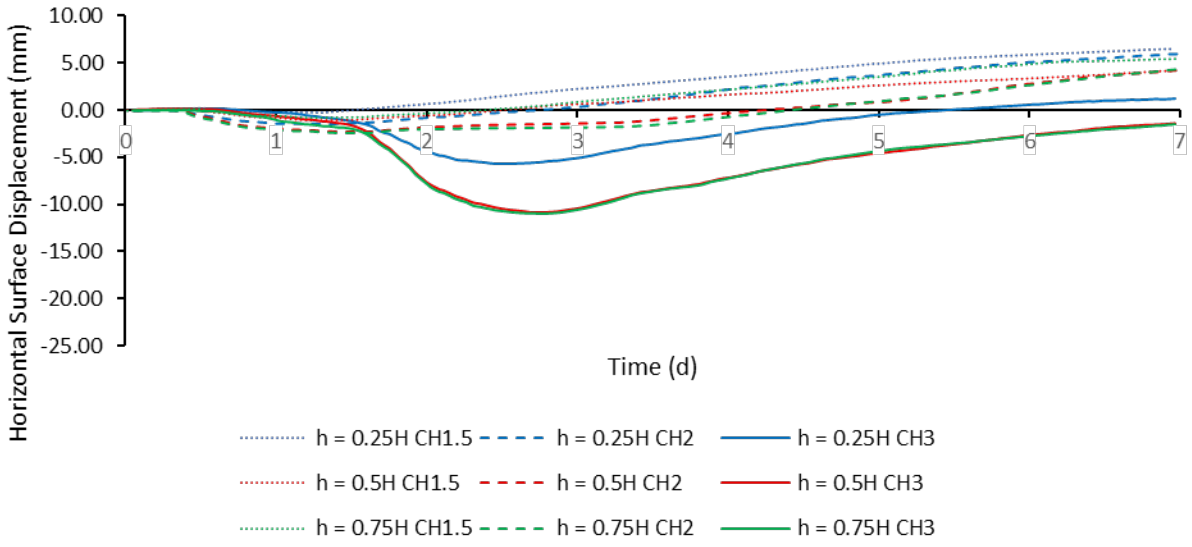

(a)

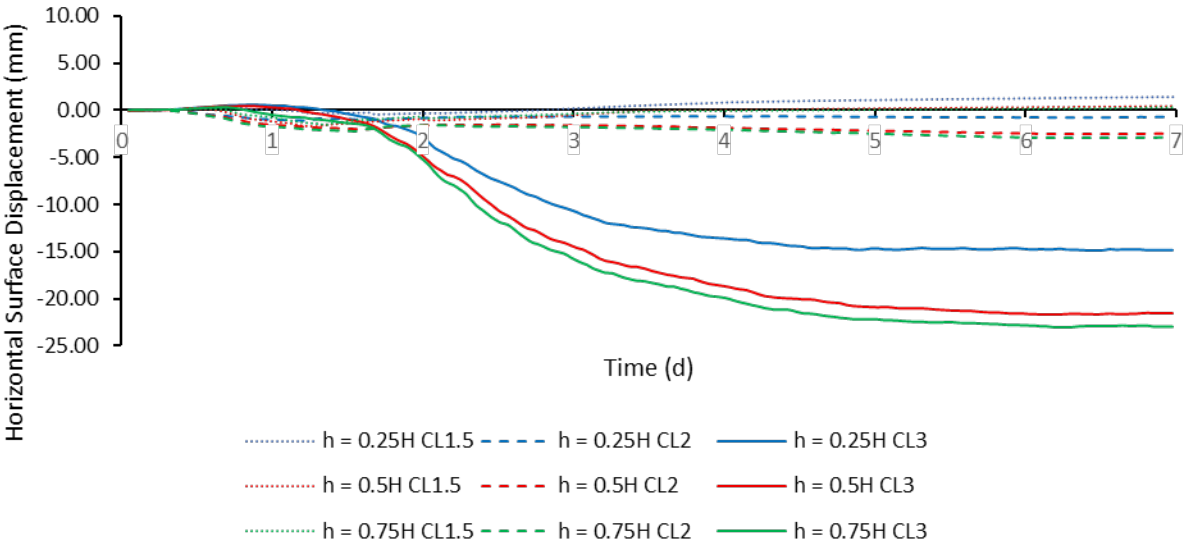

(b)

Figure 27 presents the predicted vertical surface displacement for the CH and CL embankment models as of the onset of the extreme event. Models of side slopes 3.0:1, 2.0:1, and 1.5:1 were subjected to the 7-day precipitation events of climate scenario LOS13. The figure presents the predicted displacements at three slope locations: 0.25*H*, 0.50*H*, and 0.75*H* above slope toe.

For CH embankments, shown in Figure 27a, upward vertical displacement was observed after 2–3 days as infiltration progressed to a depth of 0.5 m. This infiltration led to a wetting of the near-surface soil, which caused the soil to swell. Overall, the results indicate that swelling would likely take place in CH embankments subject to extreme events longer than 3 days. The results also indicate that swelling would likely increase with decreasing slope steepness.

For CL embankments, shown in Figure 27b, the observed displacement trends were similar to those of CH embankments. However, CL embankments did not reach near saturation conditions as CH embankments did. Therefore, unlike in CH embankments, no significant swelling displacements, if any, were observed in CL embankments during the duration of the studied extreme events. Nevertheless, CL embankments showed greater tendency to settle during extreme events than CH embankments.

Figure 27. Vertical Surface Displacement Over 7 Days at 0.25H, 0.5H and 0.75H for Side Slopes 1.5:1, 2.0:1 and 3.0:1 and Climate Scenario 13: (a) in CH Embankments; and (b) in CL Embankments

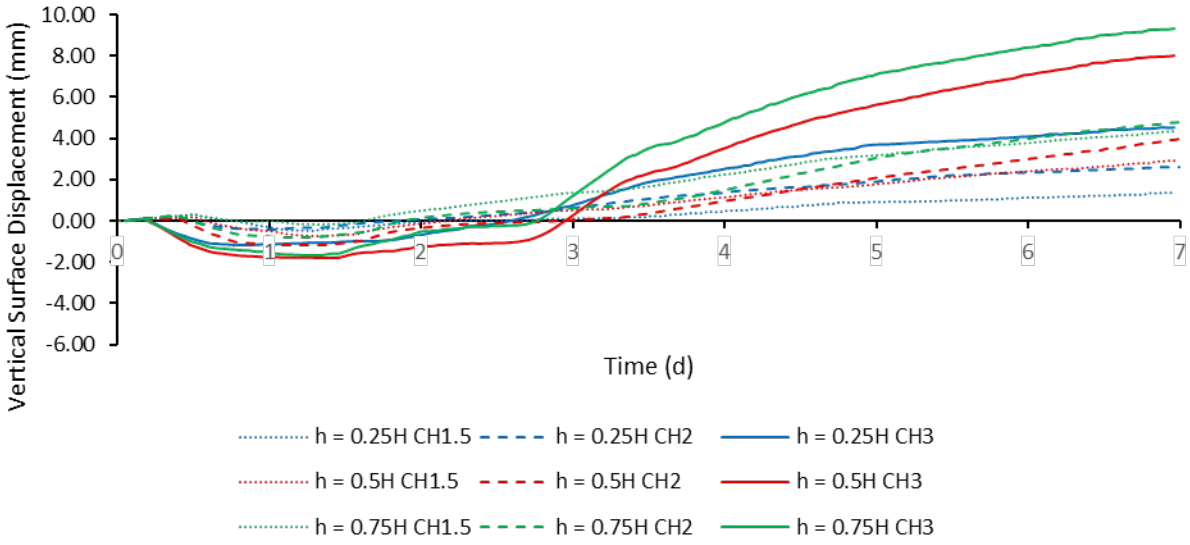

(a)

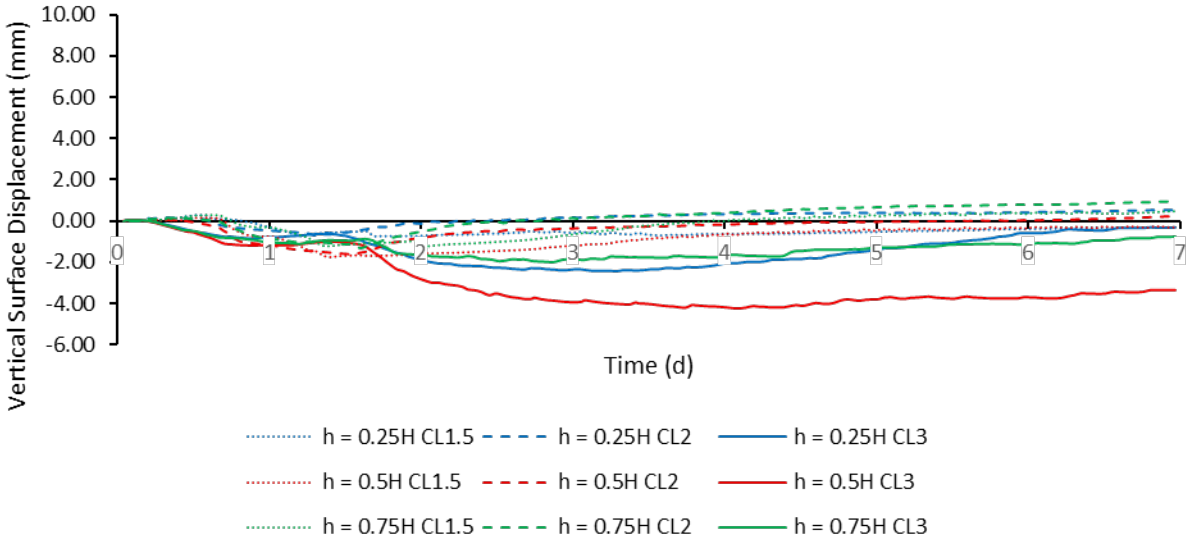

(b)

6. The Prospective Role of Performance Numerical Modeling in Geotechnical Asset Management

Geotechnical infrastructure assets include walls, slopes, embankments, and subgrades (Vessely et al., 2019). Such assets are responsible for supporting a large number of the transportation infrastructure including highways and railways. Helm et al. (2024) provided performance assessment framework based on long-term numerical modeling that could be used to improve geotechnical asset management practices. This framework has shown that numerical models can provide detailed information on asset performance (see for example Postill et al., 2021; Morsy et al., 2023a; Morsy & Helm, 2024a).

A simplified framework was adapted from Helm et al. (2024) with a focus on clay embankments studied herein, as shown in Figure 28. Specifically, the framework includes the following components:

- *Development of Geotechnical Asset Model*. This study used a numerical modeling approach previously developed by Morsy et al. (2023a, 2023b). This approach allows for simulating the construction and long-term, weather-driven hydromechanical behavior of clay embankments.

- *Validation of Geotechnical Asset Model*. The numerical modeling approach used in this study has undergone validation, demonstrating its effectiveness in capturing the long-term hydromechanical behavior of embankments (Morsy et al., 2023a, 2023b). The validation process involved a comprehensive study using a full-scale research embankment equipped with 9 years of monitoring data. Additionally, the modeling approach was validated based on its ability to predict the service life for 34 well-documented embankment failure case histories (Morsy & Helm, 2024a, 2024b).

- *Generation of Perturbed Climate*. Suites of climate perturbed parameter ensembles (PPEs) were developed by Morsy and Varela (2025) for select areas in California based on geographical climate classification. The PPEs were developed using CA DWR weather generator (Najibi & Steinschneider, 2023) and GFDL SPEAR Large Ensembles (Delworth et al., 2020).

- *Derivation of Asset-Scale Engineering Parameters*. This study derived ranges of embankment parameters for typical high plasticity clay and low plasticity clay fills, which are sensitive fills to weather-driven deterioration. The embankment geometry parameters were derived from the embankment design specifications and common practice in California (Morsy & Varela, 2025).

- *Simulation of Asset-Scale Performance*. The numerical model was used to perform a parametric evaluation to evaluate the effect of perturbed future climate scenarios on the

long-term performance of clay embankments, including the effect of average annual precipitation change, extreme precipitation quantile change, and temperature change. The evaluation involved exemplary embankments constructed from high plasticity and low plasticity clays, with varied side slopes. The simulations were performed under climate suites from 2020 through 2100. Performance indicators included near-surface soil moisture and slope displacements.

The following steps have not been completed in this current study. They are presented as part of the framework to show how the work completed herein contributes to geotechnical asset management.

- *Derivation of Network-Scale Engineering Parameter Ranges*. This step establishes ranges for asset engineering and geometry parameters within a network or an asset inventory of interest. Such information can be collected from infrastructure stakeholders with geotechnical asset management programs.

- *Development of Statistical Design for Network Assets*. This step is necessary for the subsequent development of statistical emulation. Statistical designs are necessary to ensure a comprehensive exploration of the asset parameter spaces (i.e., ranges) with minimal computational resources (Svalova et al., 2021).

- *Development of Statistical Emulation*. Predictions of long-term performance indicators obtained from the asset-scale numerical simulations could be used to train statistical emulators for long-term asset performance. An example for the development of a statistical emulator is given by Svalova et al. (2021) for cut slopes.

- *Simulation of Network-Scale Performance*. The results of the statistical emulator could be used to learn about the performance of a range of assets on a network scale. An example of network-scale performance is given by Helm et al. (2024).

Figure 28. Simplified Geotechnical Asset Management Framework for California Clay Embankments (Framework Adapted from Helm Et Al. 2024)

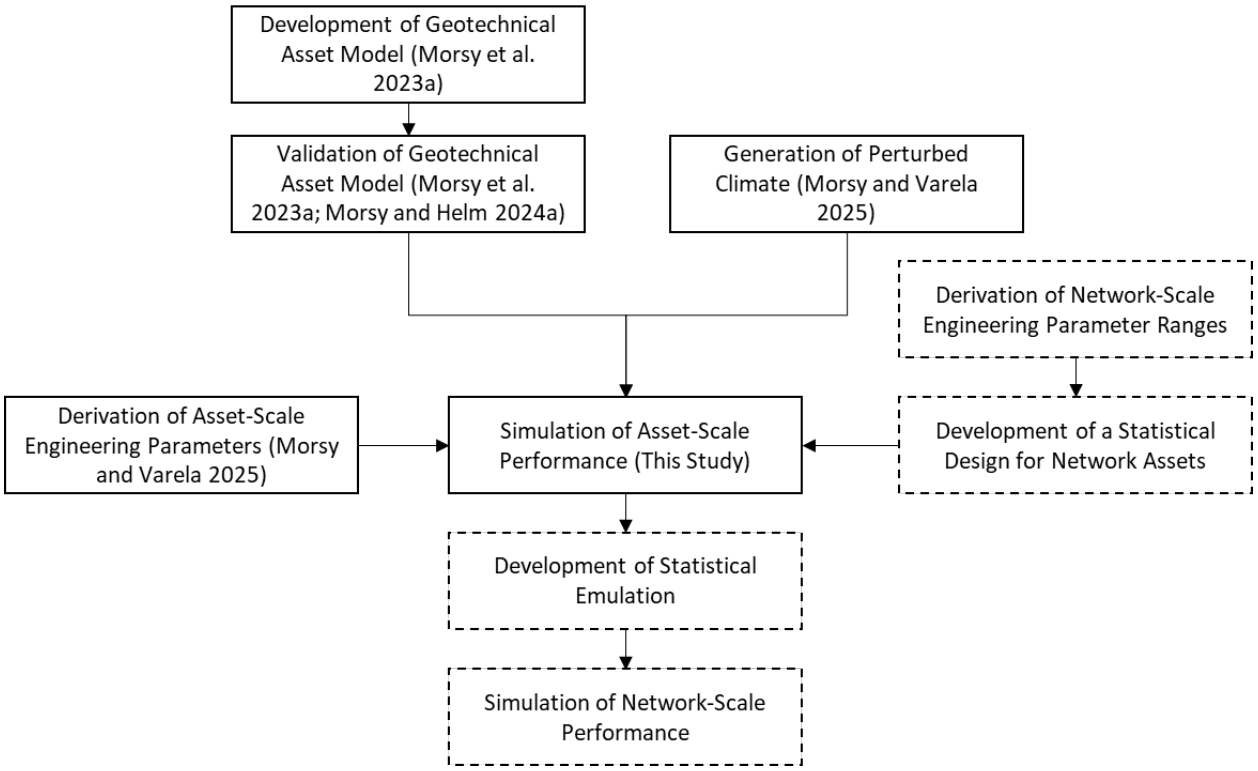

7. Summary and Conclusions

Clay embankments are susceptible to weather-related deterioration processes that can gradually compromise their stability and, in some cases, lead to unexpected failures. Climate change, along with the associated shifts in weather patterns, is projected to adversely impact the weather-related deterioration processes of transportation infrastructure, leading to exacerbated failures and/or shorter service life. Additionally, climate change is projected to increase the frequency of extreme precipitation events leading to an increase in embankment failure potential. This study evaluated (1) the effect of perturbed future climate scenarios on the long-term performance of clay embankments and (2) the effect of extreme precipitation events brought about by perturbed future climate scenarios on the hydromechanical response of clay embankments to these extreme events. A multi-phase hydromechanical geotechnical model was developed for exemplar high plasticity and low plasticity clay embankments with varied side slope angles.

A parametric evaluation was conducted to evaluate the effect of perturbed future climate scenarios on the long-term performance of clay embankments. A total of twenty-six numerical simulations were conducted in this evaluation. The following conclusions were drawn:

- The increase in future temperature is likely to lead to drier slopes and higher matric suction. For both CH and CL embankments, an approximate 9% increase was observed in the predicted near-surface matric suction as a result of +3˚C incremental change in future temperature and no change in future mean precipitation.

- The increase in future annual mean precipitation is likely to lead to wetter slopes and lower matric suction. For both CH and CL embankments, an approximate 6% decrease was observed in the predicted near-surface matric suction as a result of +12.5% incremental change in annual mean precipitation and excluding the effect of +3˚C incremental change in future temperature.

- The increase in future extreme precipitation quantile with no change in annual mean precipitation is unlikely to lead to significant long-term variation in matric suction. However, it may affect the matric suction temporarily during and after an extreme event.

- The increase in future temperature is likely to lead to smaller outward and vertical slope displacements. For CH embankments, approximately 15% decrease in the predicted mid-slope outward displacements and insignificant difference in vertical displacements were observed as a result of +3˚C incremental change in future temperature and no change in future mean precipitation. For CL embankments, an insignificant difference in predicted mid-slope outward displacements and an approximate 11% decrease in vertical displacements (swelling) were observed as a result of +3˚C incremental change in future temperature and no change in future mean precipitation.

- The increase in future mean precipitation is likely to lead to larger outward and vertical slope displacements. For CH embankments, an approximate 26% increase in the predicted mid-slope outward slope displacements and 7% increase in vertical displacements (swelling) were observed as a result of +12.5% incremental change in mean precipitation (excluding the effect of +3˚C incremental change in future temperature). For CL embankments, an insignificant difference in predicted mid-slope outward displacements and an approximate 17% increase in vertical displacements (swelling) were observed as a result of +12.5% incremental change in mean precipitation (excluding the effect of +3˚C incremental change in future temperature).

- The increase in future extreme precipitation quantile with no change in annual mean precipitation is likely to lead to larger outward and vertical (swelling) slope displacements. For CH embankments, an approximate 116% increase was observed in the predicted mid-slope outward slope displacements and a 51% increase in vertical displacements as a result of a +7% change in extreme precipitation quantile (excluding the effects of changing future annual mean precipitation and temperature). An approximate 198% increase was observed in the predicted mid-slope outward slope displacements and 96% increase in vertical displacements as a result of a +14% change in extreme precipitation quantile (excluding the effects of changing future annual mean precipitation and temperature). These results indicate that long-term irrecoverable slope deformation increases significantly with increasing the extreme event precipitation quantile, even when the annual average precipitation remains unchanged.

- As expected, steeper slopes were predicted to sustain more weather-driven deterioration over time than milder slopes leading to earlier failures. Embankments with side slopes 1.5:1 were predicted to collapse at approximately 24–40 years under various perturbed future climate scenarios. No failures were predicted in the embankments with side slopes 3.0:1 and 2.0:1 for the studied duration up to 80 years.

A parametric evaluation was conducted to evaluate the effect of extreme precipitation events brought about by perturbed future climate scenarios on the hydromechanical response of clay embankments to these extreme events. A total of fifty-four numerical simulations were conducted in this evaluation. The following conclusions were drawn:

- Future extreme rainfall events induced by perturbed future climate scenarios are likely to lead to wetter slopes and lower matric suction. CH embankments are much more susceptible damage by future extreme rainfall events than CL embankments. For CH embankments, the near-surface soil water content is likely to increase by approximately 5% as a result of a +7% change in the extreme precipitation quantile and by approximately 7% as a result of a +14% change in the extreme precipitation quantile.

- Near-surface matric suction declines during extreme precipitation events. Both CH and CL embankments are more sensitive to event duration than event intensity. CH

embankments are likely to experience irrecoverable plastic strains by 100-year extreme events that last for more than 2 days, whereas CL embankments are much less susceptible to irrecoverable plastic strains.

- Near-surface matric suction decline is likely to increase with increasing slope steepness, which makes the steeper slopes more vulnerable to failure during extreme precipitation events.

- Future extreme rainfall events are likely to increase rainfall-induced displacements in CH embankments, increasing the cumulative slope irrecoverable deformation and/or swelling-induced failures. CH embankments are likely to experience outward displacement and swelling by 100-year extreme events that last for more than 3 days. The swelling vertical displacement is likely to increase by approximately 3% as a result of a +7% change in the extreme precipitation quantile and by approximately 18% as a result of a +14% change in the extreme precipitation quantile. Unlike CH embankments, CL embankments are unlikely to experience displacements during extreme events.

Bibliography

Allen, R. G., Pereira, L. S., Raes, D., & Smith, M. (1998). *Crop evapotranspiration-guidelines for computing crop water requirements - FAO Irrigation and drainage paper 56*. Food and Agriculture Organization (FAO) of the United Nations, Rome.

Beckstrand, D., & Bunn, M. (2024). *Prevention and mitigation of surficial slope failures on fill highway embankment slopes*. NCHRP Synthesis 617, National Academies of Sciences, Engineering, and Medicine (NASEM), The National Academies Press. https://doi.org/10.17226/27645

Bedsworth, L., Cayan, D., Franco, G., Fisher, L., & Ziaja, S. (2018). *California's fourth climate change assessment. Statewide summary report.* California Governor's office of Planning and Research. Scripps Institution of Oceanography. California Energy Commission. California Public Utilities Commission.

Bishop, A.W. (1959). The principle of effective stress. *Teknisk ukeblad*, *39*, 859–63.

Caltrans (California Department of Transportation). (2005). *Caltrans pavement climate regions map*. California Department of Transportation.

Caltrans (California Department of Transportation). (2018). *Caltrans climate change vulnerability assessment summary report*. California Department of Transportation.

Caltrans (California Department of Transportation). (2020). *Highway design manual*. Seventh Edition, California Department of Transportation.

CA DWR (California Department of Water Resources). (2024). California groundwater live. Accessed June 13, 2024. https://sgma.water.ca.gov/CalGWLive/

CA DWR (California Department of Water Resources). (2015). Gridded weather generator perturbations of historical detrended and stochastically generated temperature and precipitation for the State of CA and HUC8s. Accessed January 15, 2024. https://data.ca.gov/dataset/gridded-weather-generator-perturbations-of-historical-detrended-and-stochastically-generated-te

CIMIS (California Irrigation Management Information System). (2012). *Reference evapotranspiration zones*. California Department of Water Resources (CA DWR).

Delworth, T. L., et al. (2020). SPEAR: The Next Generation GFDL Modeling System for Seasonal to Multidecadal Prediction and Projection. *Journal of Advances in Modeling Earth Systems*, *12*(3), e2019MS001895.

Fan, J., Zhang, Y., Peng, Y., et al. (2025). Study on the disaster mechanism and prevention technology of embankment slip-collapse after extreme rainfall in the loess area. *Scientific Reports*, *15*(1), 20613.

Fredlund, D. G., Rahardjo, H., & Fredlund, M. D. (2012). *Unsaturated soil Mechanics in engineering practice*. John Wiley & Sons, Inc.

Helm, P. R., Svalova, A., Morsy, A. M., et al. (2024). Emulating long-term weather-driven transportation earthworks deterioration models to support asset management. *Transportation Geotechnics*, *44*, 101155.

Itasca. (2019). *Fast Lagrangian analysis of Continua V. 8.1 – User's guide*. Itasca Consulting Group Inc.

Kovacevic, N., Hight, D. W., Potts, D. M., & Carter, I. C. (2013). Finite-element analysis of the failure and reconstruction of the main dam embankment at Abberton Reservoir, Essex, UK. *Geotechnique*, *63*, 753–767.

Kulhawy, F. H., Duncan, J. M., & Seed, H. B. (1969). *Finite element analyses of stresses and movements in embankments during construction*. U.S. Army Engineer Waterways Experiment Station.

Linacre, E. (1992). *Climate data and resources: A reference and guide*. Psychology Press.

Linrong, X., Usman, A. B., Bello, A. A. D., & Yongwei, L. (2023). Rainfall-induced transportation embankment failure: A review. *Open Geosciences*, *15*(1), 20220558.

Masson-Delmotte, V. P., Zhai, P., Pirani, S. L., et al. (2021). IPCC 2021: Summary for policymakers. In *Climate change 2021: The physical science basis*. Intergovernmental Panel on Climate Change (IPCC) Sixth Assessment Report.

Morsy, A. M. (2024). Time-to-failure prediction of fine-grained soil slopes subject to weather-driven deterioration. *Mineta Transportation Institute (MTI)*, Report No. 24-20. https://doi.org/10.31979/mti.2024.2326

Morsy, A. M., & Helm, P. R. (2024a). Failure prediction of clay embankments subject to weather-driven deterioration. *Journal of Geotechnical and Geoenvironmental Engineering*, *150*(12), 04024128.

Morsy, A. M., & Helm, P. R. (2024b). Meteorological data used in "failure prediction of clay embankments subject to weather-driven deterioration." Dataset, Newcastle University. https://doi.org/10.25405/data.ncl.26349286

Morsy, A. M., Helm, P. R., El-Hamalawi, A., et al. (2023a). Development of a multi-phase numerical modeling approach for hydromechanical behavior of clay embankments subject to weather-driven deterioration. *Journal of Geotechnical and Geoenvironmental Engineering*, *149*(8), 04023062.

Morsy, A. M., Helm, P. R., El-Hamalawi, A., et al. (2023b). Data used for "development of a multiphase numerical modeling approach for hydromechanical behavior of clay embankments subject to weather-driven deterioration." Dataset, Newcastle University. https://doi.org/10.25405/data.ncl.22144442

Morsy, A. M., & Varela, E. (2025). Evaluation of long-term performance of transportation earthworks prone to weather-driven deterioration under changing climate. *Mineta Transportation Institute (MTI)*, Report No. 25-07. https://doi.org/10.31979/mti.2025.2438

Mualem, Y. (1976). A new model for predicting the hydraulic conductivity of unsaturated porous media. *Water Resources Research*, *12*(3), 513–22.

Najibi, N., & Steinschneider, S. (2023). *A process-based approach to bottom-up climate risk assessments: developing a statewide, weather-regime based stochastic weather generator for California*. Final Report. California Department of Water Resources (CA DWR).

Nyambayo, V. P., & Potts, D. M. (2010). Numerical simulation of evapotranspiration using a root water uptake model. *Computers and Geotechnics*, *37* (1–2), 175–86.

Nyambayo, V. P., Potts, D. M., & Addenbrooke, T. I. (2004). The Influence of permeability on the stability of embankments experiencing seasonal cyclic pore water pressure changes. In *Proceedings of Advances in Geotechnical Engineering: The Skempton Conference*. pp. 898–910.

Postill, H., Helm, P. R., Dixon, N., et al. (2021). Forecasting the long-term deterioration of a cut slope in high-plasticity clay using a numerical model. *Engineering Geology*, *280*, 105912.

Potts, D. M., & Zdravkovic, L. (1999). *Finite element analysis in geotechnical engineering: theory.* Thomas Telford.

Rouainia, M., Davies, O., O'Brien, T., & Glendinning, S. (2009). Numerical modelling of climate effects on slope stability. *Proceedings of the Institution of Civil Engineers-Engineering Sustainability*, *162*, 81–89.

Samarasinghe, A. M., Huang, Y. H., & Drnevich, V. P. (1982). Permeability and consolidation of normally consolidated soils. *Journal of the Geotechnical Engineering Division*, *108*(6), 835–50.

Samtani, N. C., & Nowatzki, E. A. (2021). *Mechanically Stabilized Earth (MSE) wall fills—A framework for use of Local Available Sustainable Resources (LASR)*. Report No. FHWA-HIN-21-002. Federal Highway Administration (FHWA).

Svalova, A., Helm, P., Prangle, D., Rouainia, M., Glendinning, S., & Wilkinson, D. J. (2021). Emulating computer experiments of transport infrastructure slope stability using Gaussian processes and Bayesian inference. *Data-Centric Eng.*, *2*, e12.

Stark, T. D., Choi, H., & McCone, S. (2005). Drained shear strength parameters for analysis of landslides. *Journal of Geotechnical and Geoenvironmental Engineering*, *131*(5), 575–88.

Stirling, R. A., Toll, D. G., Glendinning, S., et al. (2021). Weather-driven deterioration processes affecting the performance of embankment slopes. *Géotechnique*, *71*(11), 957–69.

Templeton, A. E., Sills, G. L., & Cooley, L. A. (1984). Long term failure in compacted clay slopes. In *Proceedings of International Conference on Case Histories in Geotechnical Engineering*, pp. 749–54.

Vahedifard, F., Tehrani, F. S., Galavi, V., Ragno, E., & AghaKouchak, A. (2017). Resilience of MSE walls with marginal backfill under a changing climate: Quantitative assessment for extreme precipitation events. *Journal of Geotechnical and Geoenvironmental Engineering*, *143*(9), 04017056.

van Genuchten, M. T. (1980). A closed-form equation for predicting the hydraulic conductivity of unsaturated soils. *Soil Science Society of America Journal*, *44*(5), 892–98.

van Vuuren, D. P., Edmonds, J., Kainuma, M., et al. (2011). The representative concentration pathways: an overview. *Climatic Change 109*, 5–31.

Vaughan, P. R., Kovacevic, N., & Potts, D. M. (2004). Then and now: some comments on the design and analysis of slopes and embankments. In *Proceedings of Advances in Geotechnical Engineering: The Skempton Conference*, pp. 241–90.

About the Authors

Amr M. Morsy, PhD, PE

Dr. Amr Morsy is a professional civil engineer with experience in both academia and industry. His research focuses on geotechnical engineering, transportation geotechnics, environmental geotechnics, and climate adaptation. He obtained his B.Eng. and M.Sc. degrees in civil engineering from Cairo University in 2011 and 2013 respectively and obtained his PhD degree in civil engineering from The University of Texas at Austin in 2017. He worked as a postdoctoral fellow at The University of Texas at Austin in 2018 and as a practicing geotechnical engineer from 2018 to 2020. He later worked as a Research Associate at Loughborough University on the ACHILLES program grant from 2020 to 2022. He has been working as an Assistant Professor at California State University, Long Beach since 2022.

As part of his academic experience, Dr. Morsy conducts research on geotechnical infrastructure deterioration and asset management, climate change impacts on geotechnical infrastructure, and geotechnical solutions for sustainable built environments. He has excelled in physical and numerical modeling of geotechnical and geoenvironmental engineering systems, infrastructure instrumentation, and laboratory experimentation. He participated in research projects sponsored by the Transportation Research Board of the National Academies of Sciences, Engineering, and Medicine, the Engineering and Physical Sciences Research Council of the UK, the US Federal Highway Administration, the Geosynthetic Institute, and the Departments of Transportation of Texas and Indiana.

As part of his professional consulting experience, Dr. Morsy conducts rigorous analyses, designs, and forensic evaluations for a range of slopes, retaining walls, reinforced soil structures, deep excavations, bridge foundations, waste containment facilities, tailings dams, and embankment dams. He assisted expert witnesses in cases involving collapse and poor performance of earth retaining structures. He provided solutions to geotechnical problems in a number of environmental remediation projects involving cleanup of superfund sites. He conducted multi-phase flow analyses for several infrastructure features including earthworks, embankment dams, and cover systems. Some of the consulting projects he participated in served the US Environmental Protection Agency, New York State's Department of Environmental Conservation, the Departments of Transportation of New York State and Indiana, Tennessee Valley Authority, New Jersey Transit, and several other multinational private and public corporates.

Mamata Sapkota

Mamata Sapkota is a graduate student in the Department of Civil Engineering and Construction Management at California State University, Long Beach. She obtained her B.Eng. degree in civil engineering from Tribhuvan University in 2023. She is currently working as a Research Assistant at the College of Engineering.

Emma Varela

Emma Varela is a physics major in her junior year at California State University, Long Beach with a passion for the discipline and its interdisciplinary applications. Emma's academic and research experiences have allowed her to explore the intersection of physics with other fields, such as engineering and climatology, while developing technical expertise and problem-solving skills. The research she is currently contributing to utilizes climate simulations to evaluate the deterioration of earthworks, with its ultimate aim being to develop innovative solutions with lasting impacts.

Odalys Portillo

Odalys Portillo is an environmental engineering major in her junior year at California State University, Long Beach. The research she is currently contributing to utilizes climate simulations to evaluate the response of earthworks to extreme rainfall events.

MTI FOUNDER

Hon. Norman Y. Mineta

MTI BOARD OF TRUSTEES

Directors